J|A|C|S
ARTICLES
Published on Web 03/22/2003

The Involvement of Metal-to-CO Charge Transfer and Ligand-Field Excited States in the Spectroscopy and Photochemistry of Mixed-Ligand Metal Carbonyls. A Theoretical and Spectroscopic Study of $[W(CO)_4(1,2\text{-Ethylenediamine})]$ and $[W(CO)_4(N,N'\text{-Bis-alkyl-1,4-diazabutadiene})]$

Stanislav Záliš,*,† Ian R. Farrell,‡ and Antonín Vlček, Jr.*,†,‡

Contribution from the J. Heyrovský Institute of Physical Chemistry, Academy of Sciences of the Czech Republic, Dolejškova 3, CZ-182 23 Prague, Czech Republic, and Department of Chemistry, Queen Mary, University of London, Mile End Road, London E1 4NS, United Kingdom

Received July 25, 2002; Revised Manuscript Received January 17, 2003; E-mail: a.vlcek@qmul.ac.uk

Abstract: A new interpretation of the electronic spectroscopy, photochemistry, and photophysics of group 6 metal *cis*-tetracarbonyls $[M(CO)_4L_2]$ is proposed, that is based on an interplay between M → L and M → CO MLCT excited states. TD-DFT and resonance Raman spectroscopy show that the lowest allowed electronic transition of $[W(CO)_4(en)]$ (en = 1,2-ethylenediamine) has a $W(CO_{eq})_2 \rightarrow CO_{ax}$ charge-transfer character, whereby the electron density is transferred from the equatorial $W(CO_{eq})_2$ moiety to π^* orbitals of the axial CO ligands, with a net decrease of electron density on the W atom. The lowest, emissive excited state of $[W(CO)_4(en)]$ was identified as a spin-triplet $W(CO_{eq})_2 \rightarrow CO_{ax}$ CT excited state both computationally and by picosecond time-resolved IR spectroscopy. This state undergoes 1.5 ps vibrational relaxation/solvation and decays to the ground state with a ~160 ps lifetime. The ν(CO) wavenumbers and IR intensity pattern calculated by DFT for the triplet $W(CO_{eq})_2 \rightarrow CO_{ax}$ CT excited state match well the experimental time-resolved spectrum. For $[W(CO)_4(R\text{-DAB})]$ (R-DAB = *N*,*N*′-bis-alkyl-1,4-diazabutadiene), the $W(CO_{eq})_2 \rightarrow CO_{ax}$ CT transition follows in energy the W → DAB MLCT transition, and the emissive $W(CO_{eq})_2 \rightarrow CO_{ax}$ CT triplet state occurs just above the manifold of triplet W → DAB MLCT states. No LF electronic transitions were calculated to occur in a relevant energetic range for either complex. Molecular orbitals of both complexes are highly delocalized. The 5d(W) character is distributed over many molecular orbitals, while neither of them contains a predominant metal−ligand σ^* 5d(W) component, contrary to predictions of the traditional ligand-field approach. The important spectroscopic, photochemical, and photophysical roles of $M(CO_{eq})_2 \rightarrow CO_{ax}$ CT excited states and the limited validity of ligand field arguments can be generalized to other mixed-ligand carbonyl complexes.

Introduction

The rich electronic absorption spectra, photophysics, and photochemistry of mixed-ligand group 6 transition metal carbonyls $[M(CO)_4(\alpha\text{-diimine})]$ are usually interpreted in terms of low-lying M → diimine metal to ligand charge transfer (MLCT) and ligand-field (LF) electronic transitions.[1−4] The metal is an electron-rich zerovalent Cr, Mo, or W atom with a d^6 electron configuration, while α-diimine represents a N-coordinated electron-acceptor ligand that possesses low-lying π^* orbitals: derivatives of 2,2′-bipyridine (bpy), 1,10-phenanthroline (phen), 2-pyridylcarbaldehyde (R-PyCa), or 1,4-diazabutadiene (R−N=CH−CH=N−R, abbreviated R-DAB).

Electronic absorption spectra of $[M(CO)_4(\alpha\text{-diimine})]$ show a strong band in the visible region of the spectrum, whose M → diimine MLCT character is indicated by high molar absorptivity, solvatochromism, and resonance enhancement of Raman bands due to ν(CO) and diimine ν_s(CN) vibrations.[3−12] This assignment is supported by theoretical calculations on $[Cr(CO)_4(bpy)]$,[13−15] $[W(CO)_4(phen)]$,[16,17] and $[W(CO)_4(tmp)]$[16,17] (tmp = 3,4,7,8-tetramethyl-1,10-phenanthroline). The MLCT

† Academy of Sciences of the Czech Republic.
‡ University of London.

(1) Geoffroy, G. L.; Wrighton, M. S. *Organometallic Photochemistry*; Academic Press: New York, 1979.
(2) Lees, A. J. *Chem. Rev.* **1987**, *87*, 711−743.
(3) Stufkens, D. J. *Coord. Chem. Rev.* **1990**, *104*, 39−112.
(4) Vlček, A. J. *Coord. Chem. Rev.* **2002**, *230*, 225−242.
(5) Saito, H.; Fujita, J.; Saito, K. *Bull. Chem. Soc. Jpn.* **1968**, *41*, 359−364.
(6) Saito, H.; Fujita, J.; Saito, K. *Bull. Chem. Soc. Jpn.* **1968**, *41*, 863−874.
(7) Balk, R. W.; Snoeck, T.; Stufkens, D. J.; Oskam, A. *Inorg. Chem.* **1980**, *19*, 3015−3021.
(8) Wrighton, M. S.; Morse, D. L. *J. Organomet. Chem.* **1975**, *97*, 405−420.
(9) Manuta, D. M.; Lees, A. J. *Inorg. Chem.* **1986**, *25*, 1354−1359.
(10) Rawlins, K. A.; Lees, A. J. *Inorg. Chem.* **1989**, *28*, 2154−2160.
(11) Chun, S.; Getty, E. E.; Lees, A. J. *Inorg. Chem.* **1984**, *23*, 2155−2160.
(12) van Slageren, J.; Klein, A.; Záliš, S.; Stufkens, D. J. *Coord. Chem. Rev.* **2001**, *219*−*221*, 937−955.
(13) Guillaumont, D.; Daniel, C.; Vlček, A., Jr. *Inorg. Chem.* **1997**, *36*, 1684−1688.
(14) Záliš, S.; Daniel, C.; Vlček, A., Jr. *J. Chem. Soc., Dalton Trans.* **1999**, 3081−3086.

 10.1021/ja021022j CCC: $25.00

absorption band is followed at higher energies by a weaker band or a shoulder at 370−400 nm that was traditionally assigned to LF transitions, occurring between d-orbitals. This band is not solvatochromic, and its energy is nearly independent of the α-diimine ligand. The same band also occurs[5,6,10,18] in the spectra of the complexes $[M(CO)_4(en)]$, which are not expected to have any M → en MLCT transitions because the 1,2-ethylenediamine (en) ligand lacks low-lying π^* orbitals.

Multiple emission is another remarkable spectroscopic feature of $[M(CO)_4(\alpha\text{-diimine})]$ complexes. It points to the presence of several photophysically active excited states, each having a different origin.[9−11,19] The observed strongly rigidochromic, low-energy emission band has been assigned to the radiative decay of two M → diimine ^{3}MLCT excited states.[9,10] In addition, $[M(CO)_4(\alpha\text{-diimine})]$ complexes show a high-energy emission band between 530 and 550 nm (at 80 K), that is fully developed only in spectra measured using UV excitation. The same high-energy emission occurs also in the spectra of the complexes $[M(CO)_4(en)]$ (M = Mo or W)[10] and $[W(CO)_4(tmen)]$[19] (tmen = *N*,*N*,*N*′,*N*′-tetramethyl-1,2-ethylenediamine) which have no W → en MLCT states. Hence, both the emission of $[M(CO)_4(en)]$ (M = Mo, W) and the high-energy emission of $[M(CO)_4(\alpha\text{-diimine})]$ (M = Cr, Mo, or W) were previously attributed to the radiative decay of ^{3}LF excited states.[10,19]

The photochemistry of $[M(CO)_4(\alpha\text{-diimine})]$ complexes is strongly excitation-wavelength dependent. Irradiation with a UV light (≤400 nm) causes an efficient dissociation of an axial CO ligand, which is usually attributed to a prompt reaction from a dissociative LF excited state.[1,8,9] The quantum yield of photochemical CO dissociation drops sharply on increasing the irradiation wavelength into the visible spectral region, where only M → diimine MLCT transitions are excited.[4,9,20−24] In addition, M → phen ^{3}MLCT excited states of $[M(CO)_4(phen)]$ (M = Mo, W) can undergo an associative CO substitution with strong nucleophiles such as PMe_3.[4,20−22] The $[W(CO)_4(en)]$ complex, which has no W → en MLCT excited states, also undergoes photochemical CO substitution[18] whose quantum yield decreases sharply on changing the irradiation wavelength from the UV to the visible spectral region. This photochemistry has been attributed[18] to LF states, the singlets being much more reactive than the triplets.

This brief survey of experimental results suggests that electronic absorption and emission spectra as well as the photochemistry of $[M(CO)_4(\alpha\text{-diimine})]$ (M = Cr, Mo, W) complexes appear to be consistent with the presence of close-lying LF and M → diimine MLCT excited states, while the spectroscopy and photochemistry of $[M(CO)_4(en)]$ can be explained invoking low-lying singlet and triplet LF states only. Indeed, this interpretation is usually taken for granted, being used in textbooks and review articles without questions. However, several new theoretical results have emerged recently, which indicate that an interpretation based on the interplay of LF and M → diimine MLCT states in mixed-ligand metal carbonyl complexes need not be correct: (i) DFT[25−28] and CASSCF/CASPT2[29] calculations on $M(CO)_6$ (M = Cr, Mo, W) and $Ni(CO)_4$ have shown that LF excited states lie at much higher energies than was previously assumed. The lowest-lying excited states have been calculated as M → CO MLCT. Nevertheless, extension of this conclusion to mixed-ligand carbonyl complexes is not trivial because substitution of one or more CO ligands by a "weaker-field" *N*-donor is generally assumed to lower the energy of predominantly metal-d unoccupied molecular orbitals and, hence, of the LF states. (ii) Our CASSCF/CASPT2 calculations[13,15] of $[Cr(CO)_4(bpy)]$ and TD-DFT calculations[16,17] of $[W(CO)_4(phen)]$ and $[W(CO)_4(tmp)]$ have found LF-like states only at very high energies. The lowest W → diimine MLCT excited states are immediately followed in energy by several M → CO MLCT states, instead of LF states. In this respect, it should be noted that the assignment of the ca. 400 nm band of $[M(CO)_4(diimine)]$ and $[M(CO)_4(en)]$ complexes to a LF transition is contradicted by its high molar absorptivity, 1320−1700 M^{-1} cm^{-1}.[5] (iii) TD-DFT calculations[17] of triplet excited states of $[W(CO)_4(phen)]$ and $[W(CO)_4(tmp)]$ have attributed the high-energy emission to M → CO ^{3}MLCT excited states instead of ^{3}LF states because the latter were calculated to lie at far too high energies. All of these new results suggest that M → CO MLCT excited states play a very important role in the spectroscopy and photochemistry of $[M(CO)_4(\alpha\text{-diimine})]$ complexes, while the importance and occurrence of LF states is questionable. To test this hypothesis, we have carried out a theoretical and experimental study of $[W(CO)_4(en)]$ and $[W(CO)_4(R\text{-DAB})]$ complexes, Figure 1. In particular, singlet and triplet electronic transitions of both complexes were calculated by the TD-DFT technique, and their

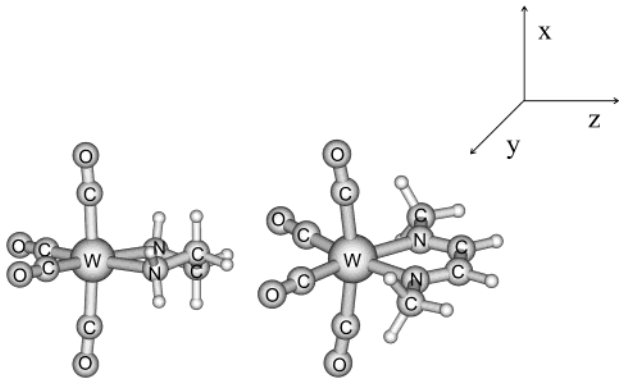

Figure 1. Molecular structures of $[W(CO)_4(en)]$ (left) and $[W(CO)_4(Me\text{-DAB})]$ (right) optimized by G98/B3LYP DFT calculations. Chosen axes orientation is shown at the right. (The calculated molecular structure of $[W(CO)_4(^i Pr\text{-DAB})]$ is very similar to that of $[W(CO)_4(Me\text{-DAB})]$.)

(15) Guillaumont, D.; Daniel, C.; Vlček, A., Jr. *J. Phys. Chem. A* **2001**, *105*, 1107−1114.
(16) Farrell, I. R.; Hartl, F.; Záliš, S.; Mahabiersing, T.; Vlček, A., Jr. *J. Chem. Soc., Dalton Trans.* **2000**, 4323−4331.
(17) Farrell, I. R.; van Slageren, J.; Záliš, S.; Vlček, A., Jr. *Inorg. Chim. Acta* **2001**, *315*, 44−52.
(18) Panesar, R. S.; Dunwoody, N.; Lees, A. J. *Inorg. Chem.* **1998**, *37*, 1648−1650.
(19) Servaas, P. C.; van Dijk, H. K.; Snoeck, T. L.; Stufkens, D. J.; Oskam, A. *Inorg. Chem.* **1985**, *24*, 4494−4498.
(20) Wieland, S.; Reddy, K. B.; van Eldik, R. *Organometallics* **1990**, *9*, 1802−1806.
(21) Fu, W. F.; van Eldik, R. *Organometallics* **1997**, *16*, 572−578.
(22) Fu, W.-F.; van Eldik, R. *Inorg. Chem.* **1998**, *37*, 1044−1050.
(23) Lindsay, E.; Vlček, A., Jr.; Langford, C. H. *Inorg. Chem.* **1993**, *32*, 2269−2275.
(24) Grevels, F.-W.; Kerpen, K.; Klotzbücher, W.; Schaffner, K.; Goddard, R.; Weimann, B.; Kayran, C.; Özkar, S. *Organometallics* **2001**, *20*, 4775−4792.
(25) Pollak, C.; Rosa, A.; Baerends, E. J. *J. Am. Chem. Soc.* **1997**, *119*, 7324−7329.
(26) Rosa, A.; Baerends, E. J.; van Gisbergen, S. J. A.; van Lenthe, E.; Groeneveld, J. A.; Snijders, J. G. *J. Am. Chem. Soc.* **1999**, *121*, 10356−10365.
(27) Baerends, E. J.; Rosa, A. *Coord. Chem. Rev.* **1998**, *177*, 97−125.
(28) Vlček, A., Jr. *Coord. Chem. Rev.* **1998**, *177*, 219−256.
(29) Pierloot, K.; Tsokos, E.; Vanquickenborne, L. G. *J. Phys. Chem.* **1996**, *100*, 16545−16550.

characters were analyzed in terms of contributing one-electron excitations and changes of electron-density distribution. Experimentally, the occurrence of low-lying M → CO MLCT transitions was explored by resonance Raman spectroscopy, while the very existence and the nature of a W → CO MLCT excited state was, for the first time, demonstrated experimentally using picosecond time-resolved IR spectroscopy. Further information on the structure and bonding in a W → CO MLCT excited state was revealed by comparing experimental and DFT-calculated excited-state IR spectra. A new model of the spectroscopy, photophysics, and photochemistry of mixed-ligand metal carbonyl complexes emerges, which stresses the role played by M → CO charge-transfer excited states.

Experimental Section

Materials. The $[W(CO)_4(^tBu\text{-}DAB)]$ and $[W(CO)_4(en)]$ complexes were synthesized using literature methods[18,30] and characterized by comparing their ^1H NMR, UV−vis, and IR absorption spectra with those published in the literature. Solvents (CH_2Cl_2 and CH_3CN) were used as obtained from Aldrich (spectrophotometric grade) and degassed by purging with dry nitrogen. KNO_3 (Merck) was used to make pellets from which resonance Raman and UV−vis reflectance spectra were measured.

Spectroscopic Measurements. Resonance Raman spectra were obtained using a Dilor XY spectrometer with a Spectra Physics 2016 Ar^+ laser. Samples were prepared as spinning rotating KNO_3 pellets or CH_2Cl_2 solutions. UV−Vis absorption spectra were measured on a Hewlett-Packard 6453 diode array spectrometer. A Perkin-Elmer Lambda 19 spectrometer equipped with a 60 mm integrating sphere was used to measure reflectance spectra of the KNO_3 pellets, which were also used for measurements of resonance Raman spectra. NMR spectra were obtained on a Bruker AM 250 MHz spectrometer.

Picosecond time-resolved IR spectra were measured using an experimental setup described in detail elsewhere.[31,32] Briefly, a Ti: sapphire regenerative amplifier, operating at a 1 kHz repetition rate, produces 800 nm pulses of an ca. 200 fs duration (fwhm).[33] This laser output is split into two. One beam is frequency-doubled to produce 400 nm, 200 fs pump pulses, while the other pumps an optical parametric oscillator that uses difference frequency generation in a $AgGaS_2$ nonlinear material to provide ca. 200 fs IR probe pulses tuneable in the "fingerprint" range 1000−3000 cm^{-1}. The wavenumber bandwidth of the IR output is 150−200 cm^{-1}. The IR beam is further split into probe and reference beams. The 400 nm pump and IR probe beams are focused to less than 200 μm diameter in the sample solution flowing through a 1 mm open jet or a variable optical path length CaF_2 flow cell, whereas the IR reference beam bypasses the sample. The relative timing of the arrival of the 400 nm pump pulses and broad-band IR probe pulses at the sample is set using an optical delay line that is placed in the pump beam optical path. The IR reference and probe beams travel by similar optical paths through two spectrometers where they are spectrally dispersed onto two Infrared Associates Inc. MCT-13-64el arrays of 64 elements each. All 128 signals from the arrays are preamplified (MCT-64000 Infrared Systems Development Corp.) and then captured by a custom-designed sample and hold analogue multiplexer system, the HX2, designed at the Rutherford Appleton Laboratory, before being read into a Datel 416J analogue-to-digital converter card inside a standard 500 MHz personal computer. The data are analyzed in pump on/pump off pairs at 1 kHz to create a rolling average of the difference IR absorbance values at each element. In this way, an ca. 150 cm^{-1} wide portion of a time-resolved IR difference absorption spectrum is obtained, which is sampled over 64 points. Broad-band spectra are then constructed by overlapping the spectra measured over several ranges. Finally, each spectrum is shown as a difference between the spectrum measured at a given time delay after excitation minus the spectrum obtained before excitation. The picosecond time-resolved IR spectra of $[W(CO)_4(en)]$, reported herein, were measured from a CH_3CN solution, which flowed through a 1 mm open jet, and excited with the 400 nm, 200 fs laser pulses.

Quantum Chemical Calculations. The ground-state electronic structures of $[W(CO)_4(en)]$ and $[W(CO)_4(R\text{-}DAB)]$ (R = ^{i}Pr, Me) complexes were calculated by density functional theory (DFT) methods using the ADF2000.02[34,35] and Gaussian 98[36] program packages. The lowest excited states of the closed shell complexes were calculated by the time-dependent DFT (TD-DFT, both ADF and G98 programs) and, for $[W(CO)_4(en)]$, also by the Configuration Interaction using Single excitations (CIS − G98) and CASSCF/CASPT2 (MOLCAS[37]) methods. Both ADF and Gaussian 98 were used for the calculations of the vibration frequencies which were performed at optimized geometries corresponding to the functional and basis set used. The IR spectrum of the $[W(CO)_4(en)]$ excited state was modeled by unrestricted Kohn−Sham calculations for the lowest lying ^3B triplet state. The electrostatic solvent influence on vibrational frequencies was modeled by polarizable continuum model (PCM) incorporated into G98.[38]

Within Gaussian 98, Dunning's polarized valence double ζ basis sets[39] were used for H, C, N, and O atoms and the quasirelativistic effective core pseudopotentials and corresponding optimized set of basis functions[40] for W. In these calculations, the hybrid Becke's three parameter functional with the Lee, Yang, and Parr correlation functional (B3LYP)[41] was used (G98/B3LYP). The comparative calculations were performed using Becke's functional half-and-half exchange mixing[42] with LYP correlation (BHandHLYP) and new hybrid spectroscopically calibrated functional B(38HF)P86,[43] which was based on mixing of 62% DF exchange with 38% of HF exchange.

The ADF program used a local density approximation (LDA) with VWN parametrization of electron gas data and functional including Becke's gradient correction[44] to the local exchange expression in conjunction with Perdew's gradient correction[45] to the LDA expression (ADF/BP). The scalar relativistic (SR) zero order regular approxima-

(30) Staal, L. H.; Terpstra, A.; Stufkens, D. J. *Inorg. Chim. Acta* **1974**, *34*, 97−101.
(31) Towrie, M.; Grills, D. C.; Matousek, P.; Parker, A. W.; George, M. W. *Appl. Spectrosc.* **2003**, *57*, 367−380.
(32) Vlček, A., Jr.; Farrell, I. R.; Liard, D. J.; Matousek, P.; Towrie, M.; Parker, A. W.; Grills, D. C.; George, M. W. *J. Chem. Soc., Dalton Trans.* **2002**, 701−712.
(33) Towrie, M.; Parker, A. W.; Shaikh, W.; Matousek, P. *Meas. Sci. Technol.* **1998**, *9*, 816−823.
(34) Fonseca Guerra, C.; Snijders, J. G.; te Velde, G.; Baerends, E. J. *Theor. Chim. Acta* **1998**, *99*, 391.
(35) van Gisbergen, S. J. A.; Snijders, J. G.; Baerends, E. J. *Comput. Phys. Commun.* **1999**, *118*, 119.
(36) Frisch, M. J.; Trucks, G. W.; Schlegel, H. B.; Scuseria, G. E.; Robb, M. A.; Cheeseman, J. R.; Zakrzewski, V. G.; Montgomery, J. A., Jr.; Stratmann, R. E.; Burant, J. C.; Dapprich, S.; Millam, J. M.; Daniels, A. D.; Kudin, K. N.; Strain, M. C.; Farkas, O.; Tomasi, J.; Barone, V.; Cossi, M.; Cammi, R.; Mennucci, B.; Pomelli, C.; Adamo, C.; Clifford, S.; Ochterski, J.; Petersson, G. A.; Ayala, P. Y.; Cui, Q.; Morokuma, K.; Malick, D. K.; Rabuck, A. D.; Raghavachari, K.; Foresman, J. B.; Cioslowski, J.; Ortiz, J. V.; Baboul, A. G.; Stefanov, B. B.; Liu, G.; Liashenko, A.; Piskorz, P.; Komaromi, I.; Gomperts, R.; Martin, R. L.; Fox, D. J.; Keith, T.; Al-Laham, M. A.; Peng, C. Y.; Nanayakkara, A.; Gonzalez, C.; Challacombe, M.; Gill, P. M. W.; Johnson, B.; Chen, W.; Wong, M. W.; Andres, J. L.; Gonzalez, C.; Head-Gordon, M.; Replogle, E. S.; Pople, J. A. *Gaussian 98*, revision A.7; Gaussian, Inc.: Pittsburgh, PA, 1998.
(37) Andersson, K.; Barysz, M.; Bernhardsson, A.; Blomberg, M. R. A.; Carissan, Y.; Cooper, D. L.; Cossi, M.; Fleig, T.; Fülscher, M. P.; Gagliardi, L.; Graaf, C. d.; Hess, B. A.; Karlström, G.; Lindh, R.; Malmqvist, P.-Å.; Neogrády, P.; Olsen, J.; Roos, B. O.; Schimmelpfennig, B.; Schütz, M.; Seijo, L.; Serrano-Andrés, L.; Siegbahn, P. E. M.; Stålring, J.; Thorsteinsson, T.; Veryazov, V.; Wierzbowska, M.; Widmark, P.-O. *MOLCAS version 5.2*; Lund University: Sweden, 2001.
(38) Amovilli, C.; Barone, V.; Cammi, R.; Cances, E.; Cossi, M.; Mennucci, B.; Pomelli, C. S.; Tomasi, J. *Adv. Quantum Chem.* **1999**, *32*, 227.
(39) Woon, D. E.; Dunning, T. H., Jr. *J. Chem. Phys.* **1993**, *98*, 1358.
(40) Andrae, D.; Häussermann, U.; Dolg, M.; Stoll, H.; Preuss, H. *Theor. Chim. Acta* **1990**, *77*, 123−141.
(41) Stephens, P. J.; Devlin, F. J.; Cabalowski, C. F.; Frisch, M. J. *J. Phys. Chem.* **1994**, *98*, 11623.
(42) Becke, A. D. *J. Chem. Phys.* **1993**, *98*, 5648.
(43) Szilagyi, R. K.; Metz, M.; Solomon, E. I. *J. Phys. Chem. A* **2002**, *106*, 2994−3007.
(44) Becke, A. D. *Phys. Rev. A* **1988**, *38*, 3098.

Table 1. Selected DFT Calculated Bond Lengths [Å] and Angles [deg] of $[W(CO)_4(en)]$ (AN = Acetonitrile)

	a^1A ground state			a^3B excited state		
	ADF/BP	G98/B3LYP	G98/B3LYP PCM–AN	ADF/BP	G98/B3LYP	G98/B3LYP PCM–AN
W−N	2.352	2.364	2.344	2.450	2.483	2.439
$W-C_{ax}$	2.035	2.048	2.049	2.039	2.048	2.045
$W-C_{eq}$	1.969	1.986	1.982	2.001	2.019	2.014
N1−C2	1.485	1.488	1.487	1.481	1.477	1.481
C2−C3	1.523	1.529	1.520	1.523	1.527	1.521
$(C-O)_{ax}$	1.171	1.169	1.164	1.173	1.165	1.165
$(C-O)_{eq}$	1.174	1.174	1.175	1.177	1.171	1.177
W−N1−C2	112.2	111.3	111.4	114.7	114.5	114.4
N1−C2−C3	109.5	109.4	109.2	108.1	108.6	108.4
N−W−N	73.6	73.9	74.1	69.0	68.6	69.5
$C_{ax}-W-C_{ax}$	171.0	174.9	176.1	174.4	174.7	176.3
$C_{eq}-W-C_{eq}$	91.1	91.0	91.7	109.9	110.8	110.9
$W-C_{ax}-O_{ax}$	174.6	176.7	176.4	178.0	177.9	179.8
$W-C_{eq}-O_{eq}$	178.6	178.2	178.4	170.9	171.3	170.3

tion[46] (ZORA) was used within ADF calculations. Slater-type orbital (STO) basis sets of triple ζ quality with polarization functions were employed. The inner shells were represented by a frozen core approximation; viz. 1s for C, N, O and 1s−4d for W were kept frozen. ADF/BP calculations were used for geometry optimization and calculations of vibrational frequencies. Compositions and energies of molecular orbitals and electronic transition energies and compositions were calculated by the asymptotically correct SAOP functional,[47] which is suitable also for higher-lying MOs and electronic transitions. Core electrons were included in ADF/SAOP calculations.

CASSCF/CAPT2 calculations used the same basis set as that used within G98 DFT calculations. The CASSCF active space for $[W(CO)_4(en)]$ includes the three highest occupied predominately 5d(W) orbitals and 13 low-lying empty orbitals involving π^*(CO) orbitals. The lowest six roots were calculated by a state-averaged procedure. The CASSCF wave functions were employed as references in subsequent CASPT2 calculations using the level shift corrected perturbation method.[48] (The effect of active-space size was investigated by performing the calculation with only eight empty orbitals. A detailed comparison is published elsewhere.[49])

The changes in the electron-density distribution upon excitation were calculated as difference electron densities between the ground state and the investigated excited state, as described by TD-DFT(G98), CASSCF/CASPT2, or CIS. The difference densities were then used to calculate differences in Mulliken population on individual molecular fragments between the ground and excited state.

The geometry optimizations were carried out without any symmetry restriction. TD-DFT calculations on $[W(CO)_4(R\text{-}DAB)]$ and $[W(CO)_4(en)]$ were performed under constrained C_{2v} or C_2 symmetry, respectively, that approximate well the optimized structures. The *z*-axis is coincident with the C_2 symmetry axis. The equatorial CO groups are located in the *yz*-plane, and the axial CO ligands lie on the *x*-axis, Figure 1. The constrained symmetries were used also for interpretation of IR spectra.

The orbital shapes and difference density plots were prepared using the Molden software.[50]

Results and Discussion

Ground-State Molecular Structures. Shown in Figure 1 are the molecular structures of $[W(CO)_4(en)]$ and $[W(CO)_4(Me\text{-}DAB)]$, optimized by G98/B3LYP DFT calculations. Selected bond lengths and angles are summarized in Table 1 and the Supporting Information, which contains also the calculated atomic coordinates. Hereinafter, the CO ligands cis and trans to the en or DAB ligand are referred to as "axial" and "equatorial", respectively. Both complexes have distorted pseudo-octahedral structures that are typical of group 6 tetracarbonyls.[4,14,16,51−55] Solvation has no significant structural effects on either species, as is documented by the nearly identical values of bond lengths and angles calculated for the complex molecules in a vacuum and in a solvent cage (Table 1). The axial W−C bonds were calculated to be significantly longer than the equatorial ones. The C≡O bond lengths are only marginally shorter for the axial than equatorial CO ligands. The axial OC−W−CO moiety is slightly bent away from the en or DAB ligand. The N−W−N bite angle is rather small, ca. 73°. As expected, the W(Me-DAB) moiety is planar, whereas W(en) is twisted, Figure 1. The optimized molecular structures of $[W(CO)_4(R\text{-}DAB)]$ (R = Me, ^{i}Pr) and $[W(CO)_4(en)]$ approximately belong to C_{2v} and C_2 symmetry point groups, respectively, that are used hereafter to describe their electronic structures and molecular vibrations. The W−N bonds are shorter for $[W(CO)_4(Me\text{-}DAB)]$ than $[W(CO)_4(en)]$ because of W-DAB π back-bonding. The slightly shorter W−C and longer C≡O bonds in $[W(CO)_4(en)]$, as compared with $[W(CO)_4(Me\text{-}DAB)]$, indicate that the W−CO π back-bonding is stronger in the en complex. Optimization of the molecular structures of both complexes using the ADF/BP technique gave results very similar to those obtained by G98/B3LYP, with the exception of W−N and $W-C_{ax}$ bond lengths which are shorter for ADF/BP. Differences between the axial and equatorial C≡O bond lengths are smaller for ADF/BP than G98/B3LYP. The experimental structures of either $[W(CO)_4(en)]$ or $[W(CO)_4(R\text{-}DAB)]$ have not been determined. Nevertheless, the calculated structural features agree well with those observed in the X-ray structures of the similar species $[W(CO)_4(MeNHCH_2CH_2NHMe)]$ and $[Mo(CO)_4(^i Pr\text{-}DAB)]$.[55,56] The axial C−M−C moiety was indeed found bent in both complexes (175.5° and 169.6°,

(45) Perdew, J. P. *Phys. Rev. A* **1986**, *33*, 8822.
(46) van Lenthe, E.; Ehlers, A.; Baerends, E. J. *J. Chem. Phys.* **1999**, *110*, 8943−8953.
(47) Schipper, P. R. T.; Gritsenko, O. V.; van Gisbergen, S. J. A.; Baerends, E. J. *J. Chem. Phys.* **2000**, *112*, 1344−1352.
(48) Roos, B. O.; Andersson, K.; Fülscher, M. P.; Serrano-Andrés, L.; Pierloot, K.; Merchán, M.; Molina, V. *J. Mol. Struct. (THEOCHEM)* **1996**, *388*, 257−276.
(49) Záliš, S.; Vlček, A., Jr.; Daniel, C. *Collect. Czech. Chem. Commun.* **2003**, *68*, 89−104.
(50) Schaftenaar, G.; Noordik, J. H. *J. Comput.-Aided Mol. Des.* **2000**, *14*, 123−134.
(51) Farrell, I. R.; Hartl, F.; Záliš, S.; Wanner, M.; Kaim, W.; Vlček, A., Jr. *Inorg. Chim. Acta* **2001**, *318*, 143−151.
(52) Jinshuan, H.; Qingrong, C.; Manfrag, W.; Meiyun, H. *Chin. J. Struct. Chem.* **1985**, *4*, 66.
(53) Jinshuan, H.; Qingrong, C.; Manfrag, W.; Shimei, L. *Chin. J. Struct. Chem.* **1985**, *4*, 69.
(54) Magomedova, N. S.; Magomedov, G. K.-I. *Metalloorg. Khim.* **1990**, *3*, 129.
(55) tom Dieck, H.; Mack, T.; Peters, K.; von Schnering, H.-G. *Z. Naturforsch.* **1983**, *38b*, 568−579.

Table 2. Selected Vibrational Frequencies of $[W(CO)_4(en)]$ and $[W(CO)_4(Me\text{-}DAB)]$ Calculated by DFT G98/B3LYP in CH_3CN and CH_2Cl_2, Respectively[a]

$[W(CO)_4(en)]$			$[W(CO)_4(R\text{-}DAB)]$		
calc. ν/cm^{-1}	expt. ν/cm^{-1}	prevailing character	calc. ν/cm^{-1}	expt. ν/cm^{-1}	prevailing character
221		δ(NWN) + δ(Wen); A	201	212[d]	δ(R-DAB) + ν(WN); A_1
402		ν(WN) + δ(Wen); A	412	433[d] ?	$\nu(WC_{ax})$; A_1
419	435[b] s	$\nu(WC_{ax})$; A	421	433[d] ?	ν(WN) + δ(R-DAB); A_1
474		$\nu(WC_{eq})$; A	464		ν(WC) + ν(WN); A_1
518	512[b] s	torsion out-of-plane $C_{eq}WC_{eq}$ + δ(Wen); A	528	531[d]	$\delta(OCWCO)_{ax}$; A_1
567	568[b] w	δ(CWC); A	595		$\delta(OCWCO)_{eq}$; A_1
			1090	1099[d]	ν(CC) + δ(CCH); A_1
1463		δ(CCH); A			
1464		δ(CCH); B			
			1506	1511[d]	ν(CN) + δ(CCH); A_1
				1482[e]	
1614		δ(CNH); B			
1619		δ(CNH); A			
1817	1811[c]	$\nu(CO)$; B_2	1860	1873[f]	$\nu(CO)$; B_2
1858	1870[c]	$\nu(CO)$; B_1	1901	1915[f]	$\nu(CO)$; A_1^1
1865	1854[c]	$\nu(CO)$; A_1^1	1904	1919[f]	$\nu(CO)$; B_1
1999	2004[c]	$\nu(CO)$; A_1^2	2006	2017[f,g]	$\nu(CO)$; A_1^2

[a] Wavenumber values were scaled using the factor of 0.961 recommended for calculation with the B3LYP functional and double-ζ basis sets.[57] The ν(CO) vibrations are described using the C_{2v} local symmetry of the $W(CO)_4$ moiety. The symbols ν, δ, and ρ indicate stretching, in-plane bending, and twisting vibrations, respectively. [b] Raman experimental wavenumbers measured from a KNO_3 pellet using 514.5 nm excitation. [c] IR experimental ν(CO) wavenumbers measured from a CH_3CN solution. Note the different order of the experimental and calculated B_1 and A_1^1 ν(CO) vibrations. [d] Raman experimental wavenumbers of $[W(CO)_4(^tBu\text{-}DAB)]$ measured from a CH_2Cl_2 solution using 514.5 nm excitation. ? means that the assignment is not unequivocal. [e] Experimental value for $[W(CO)_4(^iPr\text{-}DAB)]$ in benzene.[19] [f] IR experimental ν(CO) wavenumbers of $[W(CO)_4(^iPr\text{-}DAB)]$ measured from a cyclohexane solution.[24] [g] The corresponding Raman band of $[W(CO)_4(^tBu\text{-}DAB)]$ occurs at 2013 cm^{-1} in CH_2Cl_2.

Table 3. DFT ADF/SAOP Calculated Energies and Compositions of Selected Highest Occupied and Lowest Unoccupied Molecular Orbitals of $[W(CO)_4(en)]$ Expressed in Terms of Composing Fragments

MO	E (eV)	prevailing character	W	$(CO)_{ax}$	$(CO)_{eq}$	en
			Unoccupied			
50a	−2.72	W + en	20 (s); 6 (p_z); 13 (d_{z^2}); 20 ($d_{x^2-y^2}$)	3	3	28
46b	−2.85	W + en	12 (p_y); 19 (d_{yz})		10	53
45b	−3.18	$W + CO_{ax}$	13 (p_x); 29 (d_{xz})	48	3	7
49a	−3.24	$W + CO_{eq}$	3 (s); 2 (p_z); 9 (d_{z^2}); 7 (d_{xy}); 2 ($d_{x^2-y^2}$)	16	29	14
48a	−3.37	$W + CO_{eq}$	6 (s); 2 (p_z); 17 (d_{z^2}); 8 (d_{xy}); 6 ($d_{x^2-y^2}$)	4	43	13
47a	−3.74	en + W	2 (p_z); 9 (d_{z^2}); 2 ($d_{x^2-y^2}$)	2		83
44b	−4.06	en + W	14 (p_x); 14 (d_{xz})	5	8	54
43b	−4.19	en + W	25 (p_y); 10 (d_{yz})	4	7	50
46a	−4.34	π CO		36	60	1
42b	−4.67	$\pi\ CO_{eq}$	4 (p_x); 2 (d_{xz})	18	72	1
45a	−4.83	W + en	26 (s); 16 (p_z)	16	2	36
41b	−4.88	$\pi\ CO_{eq}$	3 (p_y); 2 (d_{yz})	21	66	4
44a	−6.14	$\pi\ CO_{ax}$	2 (s); 3 (p_z); 4 (d_{z^2})	74		13
40b	−6.32	$\pi\ CO_{ax}$	5 (p_y); 5 (d_{yz})	69	10	8
			Occupied			
43a	−8.81	$d_W + \pi\ CO_{eq}$	40 (d_{z^2}); 17 ($d_{x^2-y^2}$)	2	40	
39b	−9.14	$d_w + \pi$ CO	54 (d_{xz})	29	15	
42a	−9.19	$d_w + \pi$ CO	54 (d_{xy})	28	17	
38b	−12.60	en	4 (p_y)	2	21	72
41a	−12.65	en	4 (p_z)	2	15	77

respectively), and the NWN bite angles are rather small: 76.5°, 72.1°, respectively. The experimental W−N (2.297 Å) and both W−C (ax, 2.020 Å; eq, 1.967 Å) bond lengths in the former complex agree well with the values calculated for $[W(CO)_4$-(en)]. On the other hand, the experimental axial and equatorial CO bond lengths (1.147 and 1.161 Å, respectively) are shorter, and their difference is larger as compared with the calculated values.

DFT-Calculated Molecular Vibrations. Vibrational analysis of the $[W(CO)_4(en)]$ and $[W(CO)_4(R\text{-}DAB)]$ (R = Me or ^{i}Pr) molecules was performed using optimized molecular structures, both in a vacuum and in a solvent cage. The wavenumbers calculated by G98/B3LYP were scaled[57] by the factor 0.961. No scaling was necessary for ADF/BP values. The ν(CO) vibrations of both complexes are described herein using C_{2v} symmetry: A_1^2 (in-phase, predominantly axial CO stretch), B_1 (antisymmetric axial CO stretch), A_1^1 (out-of-phase, predominantly equatorial CO stretch), and B_2 (antisymmetric equatorial CO stretch). Computational results obtained by G98/B3LYP for selected Raman-active vibrations are summarized in Table 2.

Inclusion of solvent medium strongly influences the calculated values of the vibrational wavenumbers, affecting most the three lower-lying ν(CO) vibrations A_1^1, B_1, and B_2, which are much more separated from each other in a solvent cage than in vacuum, Table 8. Overall, the scaled G98/B3LYP vibrational wavenumbers calculated for both $[W(CO)_4(en)]$ and $[W(CO)_4$-(Me-DAB)] in a solvent cage reproduce the experimental IR

(56) Powell, J.; Lough, A.; Raso, M. *J. Chem. Soc., Dalton Trans.* **1994**, 1571−1576.

(57) Wong, M. W. *Chem. Phys. Lett.* **1996**, *256*, 391−399.

Table 4. DFT ADF/SAOP Calculated Energies and Compositions of Selected Highest Occupied and Lowest Unoccupied Molecular Orbitals of $[W(CO)_4(^i$Pr-DAB)] Expressed in Terms of Composing Fragments

MO	*E* (eV)	prevailing character	W	$(CO)_{ax}$	$(CO)_{eq}$	^{i}Pr-DAB
			Unoccupied			
$48a_1$	−2.65	^{i}Pr-DAB +W	4 (d_{z^2}); 36 ($d_{x^2-y^2}$)	5	1	52
$32b_2$	−3.19	^{i}Pr-DAB +W	2 (p_y); 31 (d_{yz})	1	6	59
$47a_1$	−3.20	^{i}Pr-DAB +W	47 (p_z); 9 (d_{z^2}); 3 ($d_{x^2-y^2}$)	5	5	50
$46a_1$	−3.31	^{i}Pr-DAB + W	9 (s); 14 (d_{z^2}); 4 ($d_{x^2-y^2}$)	2	15	47
$15a_2$	−3.63	W + CO	40 (d_{xy})	33	16	11
$25b_1$	−3.75	W + CO_{ax}	1 (p_x); 38 (d_{xz})	56	3	2
$31b_2$	−3.79	W + ^{i}Pr-DAB	40 (p_y); 6 (d_{yz})	1	1	52
$45a_1$	−3.99	W + ^{i}Pr-DAB	49 (s); 4 (p_z); 9 (d_{z^2}); 4 ($d_{x^2-y^2}$)	2	11	26
$44a_1$	−4.14	^{i}Pr-DAB	4 (s); 10 (d_{z^2}); 3 ($d_{x^2-y^2}$)		26	51
$14a_2$	−4.57	π CO		41	35	24
$13a_2$	−4.93	π * ^{i}Pr-DAB	2 (d_{xy})		30	66
$24b_1$	−5.07	π CO_{eq}	3 (p_x); 4 (d_{xz})	12	77	2
$30b_2$	−5.51	π CO_{eq}	1 (p_y)	20	76	2
$43a_1$	−6.11	π CO_{ax}	2 (p_z); 3 (d_{z^2})	89	2	1
$29b_2$	−6.39	π CO_{ax}	2 (p_y); 2 (d_{yz})	74	14	3
$23b_1$	−7.93	π * ^{i}Pr-DAB	8 (d_{xz})	14	9	68
			Occupied			
$42a_1$	−9.21	$d_W + \pi$ CO_{eq}	2 (p_z); 40 (d_{z^2}); 14 ($d_{x^2-y^2}$)	4	38	1
$12a_2$	−9.53	$d_w + \pi$ CO	49 (d_{xy})	25	18	8
$22b_1$	−9.65	$d_w + \pi$ CO	41 (d_{xz})	21	6	31
$11a_2$	−11.60	π ^{i}Pr-DAB	6 (d_{xy})	2		91
$28b_2$	−11.89	π ^{i}Pr-DAB	2 (d_{yz})		8	88

and Raman spectra much better than the vacuum-calculated values do, Table 2. Regardless of the particular computational technique (G98 or ADF) and solvent inclusion, the calculations on $[W(CO)_4$(en)] wrongly predict the $A_1{}^1$ out-of-phase ν(CO) vibration to occur at a slightly higher wavenumber than the B_1 axial ν(CO) vibration, Table 2. However, the order of the analogous vibrations of $[W(CO)_4$(Me-DAB)] is calculated correctly, $B_1 > A_1{}^1$, Table 2. The profound effect of the solvent on molecular vibrations of $[W(CO)_4$(en)] and $[W(CO)_4$(Me-DAB)] contrasts with the insensitivity of their optimized structures toward solvation, Table 1. Apparently, solvation has more influence on the shape of the potential energy surface than the position of the energetic minimum.

The R-DAB ν_s(CN) vibration, calculated for $[W(CO)_4$(Me-DAB)] in CH_2Cl_2 at 1506 cm^{-1}, gives rise to a characteristic strong peak in the resonance Raman spectrum; see below. A detailed inspection of the calculated normal coordinate reveals that the CN stretch is coupled with CH bending vibrations of both the DAB and the Me groups. A similar result was obtained previously[58] for $[W(CO)_4(^i$Pr-DAB)]. Because of this coupling, the ν_s(CN) wavenumber depends on the *N*,*N*′-substituents R.[59,60]

Generally, all of the low-frequency vibrations of $[W(CO)_4$-(R-DAB)] (R = ^{i}Pr or Me) were calculated to have a strongly coupled character, whereby skeletal metal−ligand and R−N stretches are mixed with deformations of the W(DAB) chelate ring. Therefore, both the wavenumbers and the normal coordinates are rather dependent on R. In particular, the ν_s(WN) vibration contributes to several modes. For $[W(CO)_4(^i$Pr-DAB)], the predominantly ν_s(WN) vibration was calculated in a vacuum at 575 cm^{-1}. It is strongly coupled with deformation of the whole ^{i}Pr-DAB ligand, including the ^{i}Pr substituent. Experimentally, the corresponding Raman band appears not to be resonance-enhanced. On the other hand, DFT calculation found no such vibration for $[W(CO)_4$(Me-DAB)], whose predominantly ν(WN) vibration was calculated in CH_2Cl_2 at 464 cm^{-1}. However, it is heavily coupled with ν(WC) vibrations. Previously, it was thought that the resonance-enhanced Raman band observed for various $[W(CO)_4(\alpha$-diimine)] complexes in the range 200−230 cm^{-1} corresponded to ν_s(WN).[19,59] Detailed analysis of the vibration calculated for $[W(CO)_4(^i$Pr-DAB)] in a vacuum at 218 cm^{-1} shows that this low-frequency mode is essentially a δ_s(NWN) vibration coupled with twisting of the ^{i}Pr substituent. The same vibration of $[W(CO)_4$(Me-DAB)], calculated in CH_2Cl_2 at 201 cm^{-1}, is different, involving mixed ν_s(WN) and δ(R-DAB) motions. The involvement of the motion of the *N*-substituent R in this vibration is further evidenced by its observed upward shift to ca. 270−300 cm^{-1} on going to $[W(CO)_4$(aryl-DAB)] complexes.[60] For $[W(CO)_4$(en)], the 218 cm^{-1} vibration corresponds to the NWN bending, coupled with deformation of the whole W(en) chelate ring. The ν(WN) vibration of $[W(CO)_4$(en)] was calculated at 402 cm^{-1}, close to the values reported[61] for Werner-type en complexes.

Molecular Orbitals. The energies of the Kohn−Sham molecular orbitals of $[W(CO)_4$(en)] and $[W(CO)_4(^i$Pr-DAB)], calculated by DFT (ADF/SAOP), are summarized in Tables 3 and 4, respectively, together with orbital compositions expressed in terms of contributions from the W central atom, axial and equatorial CO ligands, and the en or ^{i}Pr-DAB ligand. Generally, the MO compositions calculated using the SAOP, BP, B3LYP, BHandLYP, and B(38HF)P86 functionals are very similar. Small differences were found only in the case of some of the higher-lying unoccupied orbitals, for which SAOP is supposed[47] to give better results.

The three highest-lying occupied MOs of both $[W(CO)_4$(en)] and $[W(CO)_4(^i$Pr-DAB)] lie in an energetically narrow interval, ca. 0.4 eV wide. They can be approximately viewed as d(π) orbitals, although the d contribution does not exceed 60%. They are highly delocalized over the $W(CO)_4$ unit and, for $[W(CO)_4$-(^{i}Pr-DAB)], also over the DAB ligand. For example, the 39b

(58) van Slageren, J.; Stufkens, D. J.; Záliš, S.; Klein, A. *J. Chem. Soc., Dalton Trans.* **2002**, 218−225.
(59) Staal, L. H.; Stufkens, D. J.; Oskam, A. *Inorg. Chim. Acta* **1978**, *26*, 255−262.
(60) Balk, R. W.; Stufkens, D. J.; Oskam, A. *J. Chem. Soc., Dalton Trans.* **1982**, 275−282.
(61) Nakamoto, K. *Infrared and Raman Spectra of Inorganic and Coordination Compounds. Part B*, 5th ed.; J. Wiley & Sons: New York, 1997.

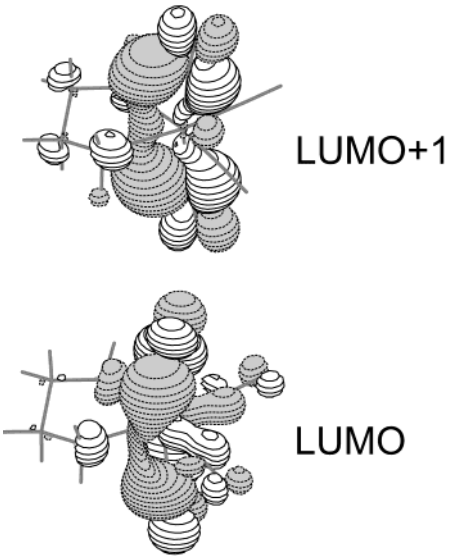

Figure 2. Shapes of the 40b LUMO and 44a LUMO+1 of $[W(CO)_4(en)]$ calculated by ADF/SAOP. (A virtually identical picture was obtained using G98/B3LYP.)

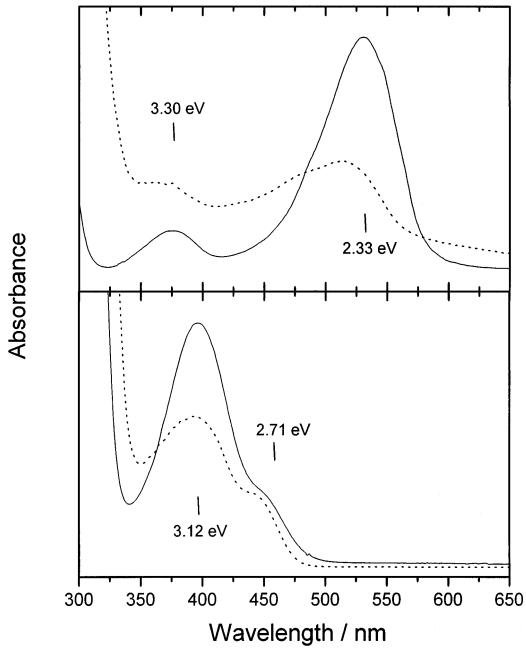

Figure 3. Absorption spectra (−) of $[W(CO)_4(en)]$ (bottom) and $[W(CO)_4(^i$Pr-DAB)] (top) measured in CH_3CN and CH_2Cl_2, respectively. Dashed curves (- - - -): diffuse reflectance spectra shown using the Kubelka−Munk function. Measured in KNO_3 pellets.

HOMO−1 of $[W(CO)_4(en)]$ contains 54% d_{xz} and 44% π^*(CO) characters. The analogous $22b_1$ HOMO−2 of $[W(CO)_4(^i$Pr-DAB)] has smaller $5d_{xz}$(W) and π^*(CO) characters (41 and 27%, respectively), while π^*(DAB) contributes 31%. This π delocalization builds up significant d(π) contributions in several unoccupied molecular orbitals that are essentially W-CO and/or W-DAB π-antibonding in character; see the 40b, 44b, 48a, or 45b orbitals of $[W(CO)_4(en)]$ (Table 3) and the $23b_1$, $25b_1$, or $15a_2$ orbitals of $[W(CO)_4(^i$Pr-DAB)] (Table 4). Remarkably, both complexes have two low-lying unoccupied MOs with predominantly axial π^*(CO) components, followed by equatorial π^*(CO) orbitals at somewhat higher energies. The axial π^*(CO) orbital is the LUMO for $[W(CO)_4(en)]$, whereas, for $[W(CO)_4(^i$Pr-DAB)], a delocalized LUMO with a principal π^*(DAB) component occurs between the HOMO and the lowest axial CO π^* orbital. In particular, the two lowest-lying unoccupied orbitals of $[W(CO)_4(en)]$, that is, the 40b LUMO and 44a LUMO+1, have a predominantly $\pi^*(y)$ and $\pi^*(z)$ axial CO character, respectively; see Figure 2. These two unoccupied axial CO π^* orbitals lie at rather low energies, 2.49 and 2.67 eV above the HOMO, respectively. The very presence of these low-lying π^*-(CO_{ax}) orbitals has important spectroscopic consequences, vide infra. A series of predominantly $\pi^*(CO_{eq})$ orbitals, which have also smaller axial $\pi^*(CO_{ax})$ contributions, follows: 41b, 42b, and 46a. In the case of $[W(CO)_4(^i$Pr-DAB)], the $23b_1$ LUMO predominantly (68%) consists of the π^*(DAB) orbital, together with smaller π^*(CO) and $5d_{xz}$(W) components. Interestingly, out of the 14% axial CO contribution, 12% originates in the $\pi^*(z)$ CO_{ax} orbital and corresponds to the W → CO_{ax} π backbonding. The remaining 2% are contributed by the out-of-phase combination of the σ orbitals of the two axial CO ligands. This is another example of a $\sigma-\pi^*$ mixing in the LUMO, which is a spectroscopically, photochemically, and electrochemically important feature of many carbonyl-diimine complexes.[4,14,16,62−65] The $23b_1$ LUMO is followed in energy by two predominantly axial CO π^* orbitals $29b_2$ and $43a_1$, that are analogous to the 40b and 44a orbitals of $[W(CO)_4(en)]$. Next in energy lie two predominantly equatorial π^* CO orbitals $30b_2$ and $24b_1$.

Contrary to the qualitative ligand-field theory arguments, DFT calculations found no unoccupied MOs with a predominant d(σ^*) component in the investigated energy range up to 6.1 eV above the HOMO. This conclusion is invariant to the functional used (SAOP, BP, B3LYP, BHandLYP, or the B(38HF)P86, which was specially optimized[43] for dd transitions). Instead, the d(σ^*) character is distributed over several different high-lying unoccupied MOs. For $[W(CO)_4(en)]$, d(σ^*) orbitals contribute to the 43b, 47a, 48a, 46b, and 50a orbitals. However, even these orbitals are rather delocalized with only minor total 5d contributions, Table 3. Moreover, they occur at too high energies to have much chemical or spectroscopic significance. The $44a_1$ orbital is the lowest unoccupied MO of $[W(CO)_4(^i$Pr-DAB)] which contains some d(σ^*) contributions. However, it lies high in energy (5.07 eV above the HOMO), containing only 13% of a d-character. Minor d(σ^*) contributions occur also in $45a_1$ and $31b_2$ MOs. The highest d(σ^*) participations, 31 and 36%, respectively, were found for $32b_2$ and $48a_1$ MOs, which lie at rather high energies.

Electronic Transitions. The electronic absorption spectrum of $[W(CO)_4(en)]$ (Figure 3, bottom) shows a band at 3.12 eV (397 nm, $\epsilon \cong 1400$ M^{-1} cm^{-1}) and a shoulder which is due to a weak band at 2.71 eV (458 nm, $\epsilon \cong 190$ M^{-1} cm^{-1}), as was determined by Gaussian analysis. Further intense absorption bands occur[5] in the UV spectral region at 4.12 eV (301 nm, 8320 M^{-1} cm^{-1}), 4.86 eV (255 nm, 28 180 M^{-1} cm^{-1}), and 5.58 eV (222 nm, 26 300 M^{-1} cm^{-1}). None of these absorption bands exhibits a solvatochromic or rigidochromic shift. The

(62) Aarnts, M. P.; Stufkens, D. J.; Wilms, M. P.; Baerends, E. J.; Vlček, A., Jr.; Clark, I. P.; George, M. W.; Turner, J. J. *Chem.-Eur. J.* **1996**, *2*, 1556−1565.
(63) Aarnts, M. P.; Wilms, M. P.; Peelen, K.; Fraanje, J.; Goubitz, K.; Hartl, F.; Stufkens, D. J.; Baerends, E. J.; Vlček, A., Jr. *Inorg. Chem.* **1996**, *35*, 5468−5477.
(64) Stufkens, D. J.; Vlček, A., Jr. *Coord. Chem. Rev.* **1998**, *177*, 127−179.
(65) Turki, M.; Daniel, C.; Záliš, S.; Vlček, A., Jr.; van Slageren, J.; Stufkens, D. J. *J. Am. Chem. Soc.* **2001**, *123*, 11431−11440.

Table 5. Selected TD-DFT Calculated Low-Lying Singlet Excitation Energies (eV) for $[W(CO)_4(en)]$ with an Oscillator Strength Larger than 0.001 (Experimental Data Obtained in CH_3CN)[a]

		ADF/SAOP	G98/B3LYP	G98/BHandHLYP	experiment
state	composition (ADF/SAOP)	transition energy (osc. str.)	transition energy (osc. str.)	transition energy (osc. str.)	energy (ext. coeff.)
a^3B	99% (43a → 40b)	2.41	2.35	2.54	2.71 (190)
a^1B	97% (43a → 40b) 2% (43a → 41b)	2.61 (0.007)	2.62 (0.011)	3.09 (0.018)	3.12 (1400)
b^1A	99% (43a → 44a)	2.72 (0.001)	2.75 (0.001)	3.02 (0.000)	
b^1B	57% (42a → 40b) 42% (39b → 46a)	3.06 (0.001)	2.95 (0.001)	3.16 (0.002)	
c^1B	31% (39b → 44a) 22% (39b → 45a) 21% (42a → 40b) 21% (42a → 41b)	3.87 (0.054)	3.63 (0.032)	4.14 (0.063)	
d^1B	88% (43a → 42b) 10% (39b → 45a)	4.22 (0.002)	4.15 (0.002)	4.44 (0.001)	4.12 (8320)
e^1B	47% (43a → 41b) 25% (42a → 42b) 10% (39b → 45a)	4.31 (0.008)	4.20 (0.023)	4.62 (0.017)	
f^1A	74% (39b → 42b) 24% (42a → 46a)	4.63 (0.007)	4.97 (0.003)	5.21 (0.001)	
f^1B	57% (43a → 44b) 32% (39b → 46a)	4.78 (0.004)	4.73 (0.004)	5.29 (0.004)	
g^1B	77% (42a → 43b) 8% (42a → 41b)	4.92 (0.032)	5.04 (0.009)	5.32 (0.003)	4.86 (28180)
g^1A	95% (43a → 47a)	5.10 (0.014)	5.06 (0.017)	5.65 (0.020)	
h^1B	95% (42a → 44b)	5.12 (0.004)			
i^1B	90% (39b → 47a)	5.39 (0.025)	5.38 (0.080)	5.76 (0.062)	5.58 (26300)
j^1B	38% (43a → 45b) 11% (42a → 43b) 10% (42a → 41b) 9% (39b → 47a)	5.53 (0.205)	5.31 (0.130)	5.80 (0.174)	

[a] The G98/B(38HF)P86 (Solomon) calculated transition energies into a^1B, b^1A, and c^1B states are 3.06 (0.016), 3.08 (0.001), and 4.29 eV (0.082), respectively.

Table 6. Changes of Mulliken Populations during the Lowest Allowed $a^1A \rightarrow a^1B$ Transition of $[W(CO)_4(en)]$ Calculated by Different Methods (Values of $(CO)_{ax}$ and $(CO)_{eq}$ Refer to the Population Changes on Each Axial and Equatorial CO Ligand, Respectively)

method	W	$(CO)_{ax}$	$(CO)_{eq}$	en
TD DFT[a]	−0.248	0.269	−0.172	0.054
TD-DFT[b]	−0.261	0.257	−0.145	0.037
TD DFT[c]	−0.367	0.337	−0.185	0.064
CASPT2[d]	−0.053	0.117	−0.078	−0.025
CIS	−0.158	0.174	−0.098	0.006

[a] TD-DFT (B3LYP). [b] TD-DFT (BHandHLYP). [c] TD-DFT (BP86). [d] CASSCF/CASPT2, large active space (6 electrons in 16 active orbitals).

spectra of $[M(CO)_4(en)]$ (M = Cr, Mo, W) are rather similar to each other with the exception of the weak band at ∼2.71 eV that was observed only for the W complex. Hence, it was attributed to a spin-forbidden transition to a triplet state.[5,8,10,18]

Shown in Table 5 are results of TD-DFT calculations of electronic transitions of $[W(CO)_4(en)]$. Comparison of the calculated and experimental data allows us to assign the shoulder at ∼2.71 eV to the lowest spin-forbidden $a^1A \rightarrow a^3B$ transition and the absorption band at 3.12 eV to the corresponding singlet transition $a^1A \rightarrow b^1B$. The calculations also revealed that these transitions originate in nearly pure 43a(HOMO) → 40b(LUMO) excitation. Inspection of the composition of these orbitals indicates that the lowest singlet and triplet transitions of $[W(CO)_4(en)]$ involve charge transfer from the W atom and the equatorial CO ligands to the axial CO ligands, further abbreviated $W(CO_{eq})_2 \rightarrow CO_{ax}$ CT. A much more detailed description of this transition is obtained from the difference electron density between the ground state and the a^1B excited state, as described by TDDFT, CASSCF/CASPT2, or CIS, see Figure 4. This way of calculating the difference densities includes the configuration mixing. The results obtained by various computational approaches are summarized in Table 6. All of these calculations reveal a large increase of electron density on the axial CO ligands, accompanied by a density decrease on the W atom and equatorial CO ligands. TD-DFT and CIS show a larger electron density decrease on W than on each CO_{eq}, in contrast with CASPT2. TD-DFT indicates a much more extensive electron density redistribution than CIS or CASPT2. Nevertheless, all of these difference density calculations support the qualitative

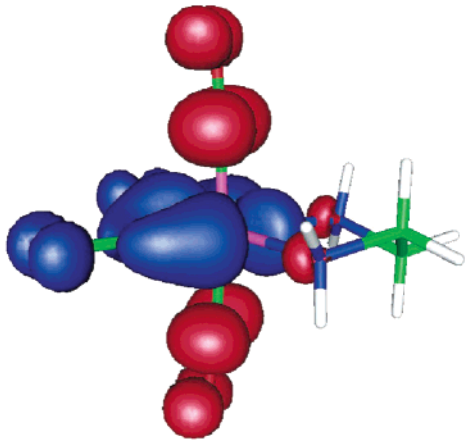

Figure 4. Change of electron density distribution upon the $a^1A \rightarrow a^1B$ electronic transition of $[W(CO)_4(en)]$. Blue and red colors correspond to a decrease and increase of electron density, respectively. Calculated from G98/B3LYP TD-DFT densities.

description of the lowest allowed $a^1A \rightarrow {}^1aB$ transition of $[W(CO)_4(en)]$ as $W(CO_{eq})_2 \rightarrow CO_{ax}$ CT (Figure 4), contradicting the previous[5,8,10,18] assignment as a LF transition.

The UV absorption bands at 4.12 and 4.86 eV are attributed to the $a^1A \rightarrow c^1B$ and $a^1A \rightarrow g^1B$ transitions, respectively. Furthermore, other close-lying transitions can contribute to these broad absorption bands; see Table 5. As is common[66] for many transition metal complexes, considerable configuration mixing occurs in higher excited states of $[W(CO)_4(en)]$. The corresponding electronic transitions are therefore composed of several one-electron excitations (Table 5), complicating their qualitative analysis based on the MOs involved. Nevertheless, it can be seen that the $a^1A \rightarrow c^1B$ transition is highly delocalized, containing a significant W → CO contribution. $a^1A \rightarrow g^1B$ is the lowest-lying transition calculated to have a partially $d(\pi) \rightarrow d(\sigma^*)$ character which arises from the 77% contribution of the 42a(HOMO−2) → 43b excitation. However, even this 42a → 43b component can hardly be regarded as the usual $d(\pi) \rightarrow d(\sigma^*)$ LF excitation, because the 42a and 43b orbitals are highly delocalized, having only 54 and 10% d-contributions, respec-

(66) Streiff, J. H.; Edwards, W. D.; McHale, J. L. *Chem. Phys. Lett.* **1999**, *312*, 369−375.

Table 7. Selected TD-DFT Calculated Low-Lying Singlet Excitation Energies (eV) for $[W(CO)_4(^iPr\text{-}DAB)]$ with Oscillator Strength Larger than 0.001 (Experimental Data Obtained in CH_2Cl_2)

		ADF/SAOP	G98/B3LYP	G98/BHandHLYP	experiment
state	composition (ADF/ SAOP)	transition energy (osc. str.)	transition energy (osc. str.)	transition energy (osc. str.)	energy (ext. coeff.)
a^1B_2	98% ($12a_2 \rightarrow 23b_1$)	1.73 (0.001)	1.77 (0.001)	2.02 (0.000)	
b^1A_1	95% ($22b_1 \rightarrow 23b_1$)	2.65 (0.162)	2.64 (0.175)	2.74 (0.209)	2.33 (6000)
b^1B_2	95% ($42a_1 \rightarrow 29b_2$)	2.90 (0.004)	3.04 (0.008)	3.41 (0.014)	
c^1A_1	97% ($42a_1 \rightarrow 43a_1$)	3.24 (0.002)	3.40 (0.001)	3.93 (0.001)	3.30 (1040)
b^1B_1	64% ($12a_2 \rightarrow 29b_2$) 33% ($22b_1 \rightarrow 43a_1$)	3.42 (0.004)	3.41 (0.007)	3.58 (0.009)	
c^1B_1	67% ($12a_2 \rightarrow 30b_2$) 22% ($22b_1 \rightarrow 43a_1$) 7% ($42a_1 \rightarrow 24b_1$)	3.96 (0.008)	4.18 (0.016)	4.51 (0.023)	*a*
c^1B_2	53% ($42a_1 \rightarrow 30b_2$) 43% ($12a_2 \rightarrow 24b_1$)	4.23 (0.016)	4.36 (0.008)	4.67 (0.007)	*a*
d^1B_2	86% ($11a_2 \rightarrow 23b_1$)	4.31(0.083)	4.91 (0.090)	5.42 (0.062)	*a*
d^1A_1	86% ($22b_1 \rightarrow 24b_1$) 5% ($12a_2 \rightarrow 13a_2$)	4.68 (0.018)			*a*
e^1A_1	68% ($12a_2 \rightarrow 13a_2$) 8% ($22b_1 \rightarrow 24b_1$) 8% ($12a_2 \rightarrow 14a_2$)	4.80 (0.048)			*a*

[a] Strong absorption above 3.75 eV was not studied in detail.

tively. In fact, the TD-DFT/SAOP calculation predicts no genuine LF electronic transition to occur in the investigated energy range up to 5.53 eV.

In conclusion, the TD-DFT ADF/SAOP calculation reproduces the $[W(CO)_4(en)]$ absorption spectrum remarkably well, although the energy of the $W(CO_{eq})_2 \rightarrow CO_{ax}$ CT lowest absorption band is somewhat underestimated. The G98/B3LYP calculation yields reasonably good transition energies but underestimates strongly the oscillator strengths of the higher transitions relative to the lowest allowed transition $a^1A \rightarrow a^1B$. The quantitative correspondence with the experimental spectrum is improved using B(38HF)LYP and, even better, BHandHLYP. Importantly, all of these calculations lead to the same qualitative conclusions that the lowest excited states are $W(CO_{eq})_2 \rightarrow CO_{ax}$ CT in nature and that no genuine LF transitions are present. These conclusions are further supported by large active space CASSCF/CASPT2 calculations. (Note that even the use of the B(38HF)LYP functional, which is optimized[43] for LF transitions, and ADF/SAOP, which is well-suitable[47] for high-lying states, did not identify any LF excited state up to very high energies.)

The electronic absorption spectrum of $[W(CO)_4(^tBu\text{-}DAB)]$ (Figure 3) shows an intense absorption band at 2.33 eV (531 nm, $\epsilon \cong 6000\ M^{-1}\ cm^{-1}$) which is due to a $W \rightarrow$ DAB MLCT transition.[59] It has a low-energy shoulder, that is especially apparent in the diffuse reflectance spectrum. A weaker, well developed, absorption band is found at 3.30 eV (376 nm, $\epsilon \cong 1040\ M^{-1}\ cm^{-1}$). This spectroscopic pattern is typical for all $[M(CO)_4(\alpha\text{-diimine})]$ complexes.[3,4,59]

The lowest-energy allowed electronic transition of $[W(CO)_4(^iPr\text{-}DAB)]$ was calculated by ADF/SAOP as $a^1A_1 \rightarrow b^1A_1$, at 2.65 eV (Table 7). It is responsible for the intense 2.33 eV absorption band of $[W(CO)_4(^tBu\text{-}DAB)]$, while the weaker $a^1A_1 \rightarrow a^1B_2$ transition (calcd at 1.73 eV) gives rise to the low-energy shoulder at ~1.89 eV. Both of these transitions are essentially single-configurational. The main $a^1A_1 \rightarrow b^1A_1$ transition originates in a predominant (95%) orbital excitation $22b_1(HOMO-2) \rightarrow 23b_1(LUMO)$, which corresponds to a partly delocalized $W \rightarrow$ DAB MLCT, in agreement with the previous empirical assignment.[3,4,7,59] This conclusion is further supported by TD-DFT(G98/B3LYP)-calculated difference densities: $-0.468\ e^-$ on W, $+0.673\ e^-$ on Me-DAB. As compared with the $M \rightarrow$ phen MLCT transition of $[W(CO)_4(phen)]$,[16,17] the $W \rightarrow$ DAB MLCT transition of $[W(CO)_4(^iPr\text{-}DAB)]$ is much more delocalized over the W(DAB) chelate ring, as follows from the comparison of the HOMO and LUMO of the two complexes. The $W \rightarrow$ DAB MLCT transitions are followed in energy by three transitions $a^1A_1 \rightarrow b^1B_2$, $a^1A_1 \rightarrow c^1A_1$, and $a^1A_1 \rightarrow b^1B_1$, all of which can contribute to the relatively weak absorption band at 3.30 eV (376 nm). The lower two transitions, $a^1A_1 \rightarrow b^1B_2$ and $a^1A_1 \rightarrow c^1A_1$ calculated at 2.90 and 3.24 eV, respectively, are virtually single-configurational, with predominant excitations directed into axial CO π^* orbitals $29b_2$ and $43a_1$, respectively. Both the $a^1A_1 \rightarrow b^1B_2$ and the $a^1A_1 \rightarrow c^1A_1$ transition have the $W(CO)_2 \rightarrow CO_{ax}$ CT character, analogous to the lowest two transitions of $[W(CO)_4(en)]$. This is demonstrated by the difference density calculated by TD-DFT(G98/B3LYP) for the $a^1A_1 \rightarrow b^1B_2$ transition of $[W(CO)_4(Me\text{-}DAB)]$: $-0.439\ e^-$ on W, $-0.166\ e^-$ on each CO_{eq}, $+0.372\ e^-$ on each CO_{ax}, and $+0.026\ e^-$ on Me-DAB. The $a^1A_1 \rightarrow b^1B_1$ transition is $W \rightarrow$ CO MLCT. It consists of two principal excitations, both being directed mostly to axial COs. As for $[W(CO)_4(en)]$, no genuine LF transitions were calculated by TD-DFT for $[W(CO)_4(^iPr\text{-}DAB)]$. In fact, no transitions with an appreciable dd character were found at energies up to 4.78 eV (260 nm), regardless of the functional used, ADF/SAOP, B3LYP, BHandHLYP, and B(38HF)P86. This conclusion is also consistent with a CASSCF/CASPT2 calculation.[49]

The emission spectrum of $[W(CO)_4(en)]$ measured[10] from an EPA glass at 80 K shows a band at 2.29 eV (542 nm), which decays with a 7.5 μs lifetime. This emission presumably occurs from the lowest triplet excited state, which was identified by TD-DFT as a a^3B $W(CO_{eq})_2 \rightarrow CO_{ax}$ CT excited state that originates almost exclusively (99%) in $43a \rightarrow 40b$ excitation. As expected, the calculated a^3B excited-state energy 2.41 eV is slightly higher than the emission band maximum energy of 2.29 eV. The emission of $[W(CO)_4(^iPr\text{-}DAB)]$ is very similar to that of $[W(CO)_4(en)]$: a single band at 555 nm (2.23 eV) that is composed of at least two emissions.[19] On the basis of TD-DFT ADF/SAOP calculations, this band was attributed to a radiative decay of two $W(CO_{eq})_2 \rightarrow CO_{ax}$ CT states b^3B_2 and b^3B_1 which originate in $42a_1 \rightarrow 29b_2$ (97%) and $12a_2 \rightarrow 29b_2$ (96%) excitations, respectively. The corresponding excited-state energies were calculated as 2.72 and 2.93 eV, respectively. $[W(CO)_4(^iPr\text{-}DAB)]$ is exceptional among $[M(CO)_4(\alpha\text{-diimine})]$ complexes because it does not show the low-lying, rigido-, and solvatochromic emission band from $W \rightarrow$ DAB MLCT excited states.[19] Three such triplet states were calculated to lie between 1.23 and 1.52 eV. The lack of low-energy emission from

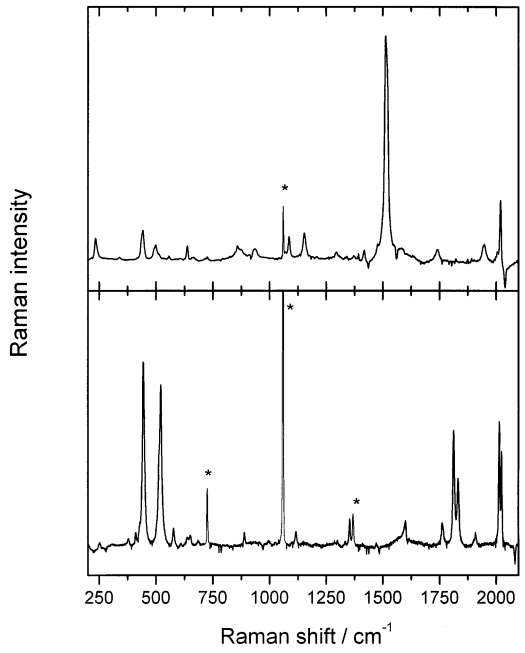

Figure 5. Raman spectra of $[W(CO)_4(^tBu\text{-}DAB)]$ (top) and $[W(CO)_4(en)]$ (bottom) measured from spinning KNO_3 pellets. Excited at 514.5 nm. Diffuse reflectance spectra of the pellets are shown in Figure 3. "*" denotes KNO_3 peaks.

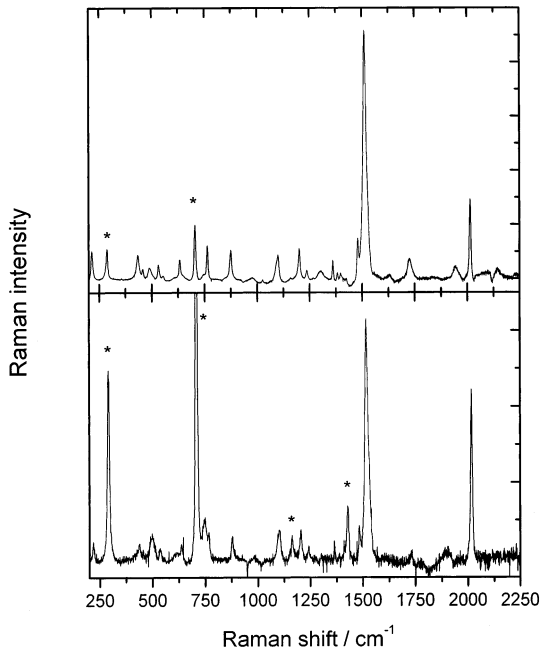

Figure 6. Raman spectra of $[W(CO)_4(^tBu\text{-}DAB)]$ measured from a spinning CH_2Cl_2 solution excited at 514.5 nm (top) and 458 nm (bottom).

$[W(CO)_4(^iPr\text{-}DAB)]$ was explained[19] by the very fast decay of the W → DAB MLCT states.

The present triplet TD-DFT calculations clearly discard the traditional assignment of the emission of both $[W(CO)_4(en)]$ and $[W(CO)_4(^iPr\text{-}DAB)]$ to LF states. For the former complex, no LF triplet excited state was calculated in the investigated energy range up to 5.37 eV, using triplet TD-DFT G98/B3LYP.

Resonance Raman Spectroscopy. The DFT-based conclusion about the predominant $W(CO_{eq})_2 \rightarrow CO_{ax}$ MLCT character of the 396 and 458 nm bands of $[W(CO)_4(en)]$ and the 376 nm band of $[W(CO)_4(^iPr\text{-}DAB)]$ was qualitatively tested by resonance Raman spectroscopy. Shown in Figure 5 are Raman spectra of both complexes measured from spinning KNO_3 pellet using excitation at 514.5 nm. The spectrum of $[W(CO)_4(en)]$ exhibits two strong doublets at 2006/2017 cm^{-1} and 1803/1823 cm^{-1} which are attributed, by comparison with the IR spectrum, to the A_1^2 and B_2 ν(CO) vibrations, respectively. The splitting seems to be due to solid-state effects. The low-wavenumber region is dominated by two peaks at 435 and 512 cm^{-1}. On the basis of DFT calculations (Table 2), the 435 cm^{-1} peak was assigned to the $\nu(WC_{ax})$ A_1 vibration. The peak at 512 cm^{-1} and the very weak band at 568 cm^{-1} probably belong to a torsional vibration of the equatorial $(OC)_2W(en)$ moiety and a δ(CWC) vibration of the whole $W(CO)_4$ moiety, respectively.

The intensity of the ν(CO) bands relative to the 1358 cm^{-1} KNO_3 peak slightly increases on changing the excitation wavelengths from 514.5 to 488.1 nm. The ν(CO) peaks are prominent even in the spectrum excited at 458 nm, but measurement of quantitative excitation profiles was prevented by a strongly wavenumber-dependent reabsorption of the Raman scattered light in the spectral region of the edge of the $[W(CO)_4(en)]$ absorption, Figure 3. The observed increase of Raman band intensities as the excitation wavelength approaches the 3.12 eV (397 nm) absorption band is indicative[67] of a preresonance enhancement from the lowest allowed transition, that is, $a^1A \rightarrow a^1B$. The (pre)resonance Raman spectra show that the largest distortions of the $[W(CO)_4(en)]$ molecule upon excitation take place along the normal coordinates responsible for the 435 and 512 cm^{-1} bands which have the highest intensities *and* occur at relatively low wavenumbers. This means that the $W-C_{ax}$ bonds and the overall geometry of the equatorial $(OC)_2W(en)$ moiety are most affected by excitation. The C≡O bonds are influenced as well, but to a lesser extent. This observation is in line with the proposed $W(CO_{eq})_2 \rightarrow CO_{ax}$ CT character of the $a^1A \rightarrow a^1B$ electronic transition responsible for the 3.12 eV band and agrees with the calculated structural changes; see Table 1. The $W(CO_{eq})_2 \rightarrow CO_{ax}$ CT transition is expected to affect the C≡O and W−C bonds and the equatorial CWC moiety through the π-electron density redistribution, while the W(en) bonding is influenced by the decrease of the electron density on the W atom. The occurrence of the resonance-enhanced Raman band due to the B_2 vibration is highly unusual. It is most likely caused by a solid-state distortion that removes symmetry restrictions. Alternatively, it could be due to a B-term scattering[67] resulting from a coupling of two electronic states of A and B symmetries through the B_2 vibration.

The resonance Raman spectrum of $[W(CO)_4(^tBu\text{-}DAB)]$ measured from a KNO_3 pellet shows a very strong peak at 1505 cm^{-1} due to the ν(CN) vibration of the DAB ligand and a A_1^2 ν(CO) peak at 2011 cm^{-1}. In addition, it contains the following weaker peaks: 224, 433, 489, 628, 1077, and 1143 cm^{-1}, Figure 5. (The peak at 1936 cm^{-1} is a solid-state artifact, absent in the solution spectrum. Its wavenumber does not correspond to any of the ν(CO) vibrations.) The spectrum measured from a CH_2Cl_2 solution (Figure 6) shows strong ν_s(CN) and A_1^2 ν(CO) peaks at 1511 and 2013 cm^{-1}, respectively, together with much weaker peaks at 212, 433, 457(vw), 488, 531, 632, 763, 874, 1099, 1201, 1236(vw), 1360, and 1479 cm^{-1}; see Table 2 for the DFT-based vibrational assignment. This resonance Raman

(67) Clark, R. J. H.; Dines, T. J. *Angew. Chem., Int. Ed. Engl.* **1986**, *25*, 131−158.

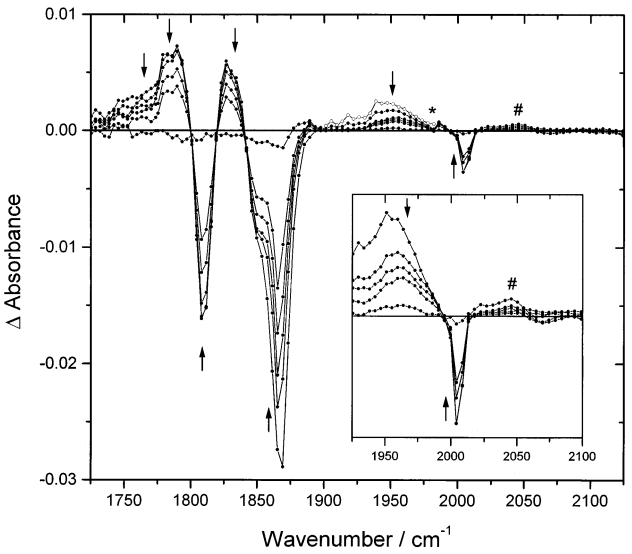

Figure 7. Picosecond time-resolved IR spectrum of $[W(CO)_4(en)]$ in CH_3CN solution. Spectra measured at the time delays of 1, 2, 8, 20, 50, 100, 1000 ps after excitation with a 400 nm, ca. 200 fs laser pulse are shown in the order specified by the arrows. Each spectrum is presented as a difference of the spectra obtained after and before excitation. The negative peaks correspond to the bleached ground-state absorption, whereas the IR bands due to the photoproduced transient are shown as positive. ○: Spectrum measured at 1 ps. Only the 1900 and 1982 cm^{-1} range is shown for clarity. ●: Spectra measured at 2, 8, 20, 50, 100, and 1000 ps. *: Artifact caused by joining spectra measured in different windows. #: The weak signal between 2030 and 2080 cm^{-1} appears to be an artifact. Its intensity sharply falls between 2 and 5 ps and then behaves randomly. Inset: Detail of the high-frequency region measured in the same spectral window. Spectra obtained at 2, 8, 50, 100, and 1000 ps are shown in the direction of the arrows.

spectral pattern is mostly determined by the allowed W → DAB MLCT transition at 530 nm, as is documented by the strong enhancement of the ν_s(CN) peak. An enhancement of the peaks due to other DAB vibrations and various skeletal and deformation modes is in line with the partial delocalization of this transition over the W(DAB) chelate ring.[3,19] Notably, the ratio of the intensities of the ν(CO) and ν_s(CN) peaks increases from 0.3 to 0.6 on changing the excitation wavelength from 514.5 to 458 nm, that is, away from the resonant W → DAB MLCT transition and toward the 376 nm band; see Figures 6 and 3. This relative intensity change cannot be caused by reabsorption which should have exactly the opposite effect; see Figure 3. Hence, this increase of the relative intensity of the ν(CO) band can be attributed to a resonance enhancement from the 376 nm absorption band, providing evidence for the $W(CO_{eq})_2 \rightarrow (CO_{ax})$ character of the underlying electronic transitions.

Structure and Dynamics of the Lowest a^3B Excited State of $[W(CO)_4(en)]$: Picosecond Time-Resolved Infrared Spectroscopy and DFT Calculations. Shown in Figure 7 are the time-resolved difference IR spectra measured at selected time delays after excitation of $[W(CO)_4(en)]$ in a CH_3CN solution with a 400 nm, ~200 fs (fwhm) laser pulse. The negative peaks are due to the bleached ground-state absorption, while the broad positive absorption belongs to photoproduced transient species. Both of these features are fully developed within the time resolution of the experiment, that is, less than 1 ps. The bleach recovery is almost complete, excluding any irreversible photochemistry. This is in agreement with the low (0.05) photochemical quantum yield of $[W(CO)_4(en)]$ photodecomposition under 405 nm irradiation.[18] All of the spectral features decay with the same kinetics (vide infra), demonstrating that only a single transient species is present, which decays directly and nearly quantitatively back to the ground state. These observations allow us to attribute the transient IR absorption to the lowest-lying excited state of $[W(CO)_4(en)]$, which was identified above by TD-DFT as the a^3B $W(CO_{eq})_2 \rightarrow CO_{ax}$ CT excited state.[68]

Detailed analysis of the time-resolved spectra is complicated by a strong overlap between the transient and bleached spectral features in the region below 1900 cm^{-1}, Figure 7. To obtain the excited-state IR band maxima, the 8 and 50 ps time-resolved difference spectra were corrected for the bleached ground-state absorption by a numerical addition of the ground-state spectrum whose intensity was scaled commensurately to the intensity of the bleached 1865 cm^{-1} peak; see Supporting Information. It follows that the $[W(CO)_4(en)]$ in its a^3B excited state has ν(CO) IR bands at ca. 1960 cm^{-1} (weak, very broad) and approximately at 1873 cm^{-1} (strong), 1824 cm^{-1} (medium), and 1793 cm^{-1} (weak, tailing to ca. 1740 cm^{-1}). All of the IR bands are rather broad, as can be expected for a CT excited state.[69] The highest band at ca. 1960 cm^{-1} can be straightforwardly attributed to the in-phase A_1^2 ν(CO) mode. The pattern of the lowest three bands is rather uncharacteristic for a C_{2v} *cis*-tetracarbonyl species because they are well separated and the lowest band at 1793 cm^{-1} seems to have the lowest intensity. This intensity pattern suggests that the 1793, 1824, and 1873 cm^{-1} bands belong to the out-of-phase A_1^1, B_2, and B_1 ν(CO) vibrations, respectively. The unusual shift of the A_1^1 vibration below B_2 is well reproduced by DFT calculations; see below. The A_1^2 and A_1^1 bands are strongly shifted to lower wavenumbers relative to the corresponding bands of the ground state, whereas the wavenumbers of the B_2 and B_1 vibrations are nearly unchanged. The decrease of the average ν(CO) wavenumber on excitation indicates an increase of population of π^*(CO) orbitals that weakens C≡O bonds. The change of the order of the ν(CO) modes points to a major structural reorganization of the $W(CO)_4$ moiety and redistribution of electron density between the CO ligands. This conclusion is in a qualitative agreement with the $W(CO_{eq})_2 \rightarrow CO_{ax}$ CT character of the a^3B excited state.

ADF/BP and G98/B3LYP DFT calculations were used to calculate the optimized structure of $[W(CO)_4(en)]$ in its a^3B excited state and simulate its IR spectrum. Data in Table 1 show that the most dramatic structural differences between the a^1A ground and a^3B excited state concern the bond angle in the equatorial $(OC)_2W(en)$ moiety. The $C_{eq}-W-C_{eq}$ angle opens by 20°, and the NWN bite angle decreases by 8°. At the same time, the $W-C_{eq}$ and W−N bonds elongate. The axial and equatorial C≡O bonds slightly lengthen and shorten, respectively, in accord with the expected electron density shift. Interestingly, excitation causes the equatorial W−C−O units to bend by 7−8°. The comparison between calculated and experimental excited-state ν(CO) wavenumbers is shown in Table 8. It follows that the wavenumbers calculated for the a^3B excited state of solvated $[W(CO)_4(en)]$ agree well with experimental values, supporting the assignment of the experimental spectrum to the a^3B state. Data in Table 8 show that the ν(CO)

(68) The alternative assignment of this transient to $[W(CO)_4(N\text{-en})]$ in which one of the W−N bonds is photolytically opened is unlikely because (i) chelate-ring closure is expected to be much slower than 150 ps and (ii) the ν(CO) vibrations should shift to higher wavenumbers from their ground-state values because of the loss of a strong electron donation from one of the N donor atoms of en.

(69) Turner, J. J. *Coord. Chem. Rev.* **2002**, *230*, 212−223.

Table 8. Comparison of the Wavenumbers of ν(CO) Vibrations of the Ground State and the Lowest Triplet Excited State of [W(CO)$_4$(en)] Calculated by ADF/BP and G98/B3LYP[a]

a^1A ground state				a^3B excited state			
ADF/BP vacuum	G98/B3LYP vacuum	G98/B3LYP acetonitrile	exp.	ADF/BP vacuum	G98/B3LYP vacuum	G98/B3LYP acetonitrile	exp.
1872 (B_2)	1873 (B_2)	1818 (B_2)	1811	1842 (A_1^1)	1860 (A_1^1)	1811 (A_1^1)	1793[b]
1878 (B_1)	1878 (B_1)	1858 (B_1)	1870	1856 (B_2)	1877 (B_2)	1826 (B_2)	1824[b]
1891 (A_1^1)	1892 (A_1^1)	1865 (A_1^1)	1854	1860 (B_1)	1892 (B_1)	1862 (B_1)	1873[b]
1989 (A_1^2)	1994 (A_1^2)	1999 (A_1^2)	2004	1952(A_1^2)	1979 (A_1^2)	1973 (A_1^2)	1960[c]

[a] Values in cm^{-1}. Vibrations are described using the C_{2v} local symmetry of the W(CO)$_4$ moiety. G98/B3LYP calculated values were scaled by the factor of 0.961 recommended for DFT calculations with double-ζ basis sets.[57] Note that the unscaled ADF/BP ν(CO) wavenumbers are very close to the scaled G98/B3LYP values for the ground but not the excited state. [b] Estimated from the time-resolved IR spectrum corrected for overlapping bleached ground-state absorption. [c] Estimated maximum of a broad band in the time-resolved IR spectrum.

wavenumbers obtained by G98/B3LYP in a vacuum are too high and the difference between the ground- and excited-state A_1^2 wavenumbers is too low (-15 cm^{-1}) in comparison with the experimental shift of -44 cm^{-1}. The values obtained by an ADF-vacuum calculation are much more reasonable than the G98/B3LYP-vacuum ones. The ADF/BP calculated shift of the A_1^2 vibration is -37 cm^{-1}, close to the experiment, although the wavenumbers of the A_1^1, B_2, and B_1 vibrations are again calculated too high and too close together. The agreement between calculated and experimental ν(CO) wavenumbers improves significantly when the solvent is included into the calculations. The G98/B3LYP calculation in a CH_3CN cavity still underestimates the shift of the A_1^2 vibration on excitation (-20 cm^{-1}) but reproduces much better the wavenumbers and splitting between the lower A_1^1, B_2, and B_1 vibrations than the vacuum calculations, Table 8. Notably, all calculations predicted the unusual order of the wavenumbers of the three lowest ν(CO) vibrations: $A_1^1 < B_2 < B_1$, in agreement with the experiment. The good correspondence between the calculated and experimental excited-state ν(CO) vibrations supports the assignment of the lowest excited state of [W(CO)$_4$(en)] as W(CO$_{eq}$)$_2$ $\rightarrow$ (CO$_{ax}$) and indicates that the calculated excited-state structure (see above and Table 1) is also close to reality.

The time-resolved IR spectra also reveal the dynamics of the a^3B excited state. Its decay is biexponential with lifetimes of 1.5 ± 0.5 and 156 ± 20 ps. The initial, 1.5 ps, process is manifested by a small upward shift and narrowing of the high-wavenumber band at 1960 cm^{-1} band that occurs between 1 and 5 ps and a change in the intensity ratio of the 1868 and 1810 cm^{-1} bleached ground-state bands from ca. 2.0 at 1 ps to 1.2 at 50 ps. The ratio between the corresponding ground-state IR bands is 1.55. The change of the bleach peak intensity ratio with time indicates that an overlapping transient absorption moves to higher wavenumbers, apparently accompanied by a growth of an absorption band at around 1870 cm^{-1}. This band overlaps with the ground-state 1870 cm^{-1} band, diminishing its negative intensity at later times. The blue shift of the excited-state IR bands between 1 and ca. 5 ps indicates that this early spectral evolution is caused by vibrational relaxation and solvation of the a^3B excited state.[70−72] The predominant ~160 ps component corresponds to a nonradiative decay to the ground state, as is manifested by the identical kinetics of the bleach recovery.

Finally, it should be noted that the very observation of a defined IR spectrum of the a^3B excited state and of its vibrational relaxation shows that the potential energy surface of the a^3B state is bound, with a defined minimum and equilibrium geometry. Hence, the a^3B excited state is expected to be essentially unreactive. This conclusion is supported by the very low quantum yield (0.007) of CO substitution by CH_3CN measured under irradiation at 458 or 476 nm.[18] The observation[10] of a low-temperature emission from the a^3B state is also in line with its bound character. Any CO dissociation is thus expected to occur from singlet excited states, in competition with intersystem crossing into the lowest a^3B state.

Concluding Remarks

The theoretical and experimental results discussed above change our view of the electronic spectroscopy and photochemistry of group 6 metal *cis*-tetracarbonyls [M(CO)$_4$L$_2$] and, upon generalization, of mixed-ligand carbonyl complexes at large. The traditional, textbook, picture is based on the presence of low-lying MLCT and LF excited states derived from M(dπ) $\rightarrow$ π*(ligand) and d(π) $\rightarrow$ d(σ*) excitations, respectively.[1] The lowest excited state was supposed to be either MLCT or LF, depending on the π-acceptor strength of the hetero-ligand. The M $\rightarrow$ CO MLCT excited states were believed to lie at higher energies, manifested by strong electronic transitions deep in the UV spectral region. Emission and photochemistry of substituted metal carbonyl complexes were attributed to MLCT and/or LF excited states.[3,8−11,18] Herein, it is argued that the presence of low-lying M(CO$_{eq}$)$_2$ $\rightarrow$ CO$_{ax}$ CT excited states is a common feature of mixed-ligand tetracarbonyl complexes *cis*-[M(CO)$_4$L$_2$], M = Cr, Mo, or W. Their spectroscopy, photophysics, and photochemistry can thus be interpreted by an interplay between M $\rightarrow$ L MLCT and M(CO$_{eq}$)$_2$ $\rightarrow$ CO$_{ax}$ CT excited states. Complexes with π electron-accepting ligand (L$_2$ = α-diimine or L = 4-X-pyridine; X = CN, CHO, Cl, etc.) have the lowest excited state M $\rightarrow$ L MLCT, which is closely followed in energy by M(CO$_{eq}$)$_2$ $\rightarrow$ CO$_{ax}$ CT excited states. The latter becomes the lowest excited state if L is an electronically saturated ligand, lacking low-lying unoccupied π* orbitals, such as L$_2$ = en and other diamines or L = pyridine, 4-R-py, and, presumably, also phosphines. The nature of the lowest excited state corresponds to the LUMO character: [M(CO)$_4$(en)], M = Cr, Mo, W; analogous complexes with diamine ligands have a predominantly axial CO π* LUMO, while the [M(CO)$_4$(α-diimine)] complexes have a predominantly π*(diimine) LUMO.

Virtually all [M(CO)$_4$(α-diimine)] complexes α-diimine = bpy, phen, R-DAB, or pyridine-carbaldehyde (R-PyCa), as well

(70) Asbury, J. B.; Wang, Y.; Lian, T. *Bull. Chem. Soc. Jpn.* **2002**, *75*, 973−983.
(71) Dougherty, T. P.; Heilweil, E. J. *Chem. Phys. Lett.* **1994**, *227*, 19−25.
(72) Dougherty, T. P.; Grubbs, W. T.; Heilweil, E. J. *J. Phys. Chem.* **1994**, *98*, 9396−9399.

as $[M(CO)_4(X\text{-}py)_2]$, show a weak absorption band between 3.44 and 3.10 eV (360−400 nm), above the strong M → diimine MLCT band.[3−6,8−11,59,73,74] Previously, the 3.44−3.10 eV (360−400 nm) band was always attributed to a LF transition. For $[W(CO)_4(en)]$ and $[W(CO)_4(^i\text{Pr-DAB})]$, this band occurs at 3.12 and 3.30 eV, respectively, and was reassigned herein to $W(CO_{eq})_2 \rightarrow CO_{ax}$ CT transition(s), using theoretical and spectroscopic (resonance Raman) arguments. Generalization of these results, together with our calculations on $[M(CO)_4(phen)]$ (M = Cr, W)[16,17] and $[Cr(CO)_4(bpy)]$,[15] allow us to conclude that the $M(CO_{eq})_2 \rightarrow CO_{ax}$ transition is ubiquitous in group 6 metal *cis*-tetracarbonyls and responsible for the 3.44−3.10 eV (360−400 nm) band.

This reinterpretation of the electronic excited states and absorption spectra also requires us to change our view of the photophysics and photochemistry of *cis*-tetracarbonyls of Cr, Mo, and W. The lowest-lying excited state of $[W(CO)_4(en)]$ was identified as the spin-triplet a^3B $W(CO_{eq})_2 \rightarrow CO_{ax}$ CT state, whose radiative decay is manifested by a long-lived (7.5 μs) emission observed from $[W(CO)_4(en)]$ in low-temperature glasses.[10] The solution lifetime of the $W(CO_{eq})_2 \rightarrow CO_{ax}$ CT state of $[W(CO)_4(en)]$ is much shorter, ca. 160 ps, while the quantum yield of the CO photosubstitution in $[W(CO)_4(en)]$ measured using excitation into the lowest spin-forbidden $a^1A \rightarrow a^3B$ $W(CO_{eq})_2 \rightarrow CO_{ax}$ CT absorption band is very low, ca. 0.007.[18] At the same time, the IR spectrum and DFT structure optimization show that the a^3B state is bound, with a defined energetic minimum on its potential energy surface. Hence, it is supposed that the a^3B $W(CO_{eq})_2 \rightarrow CO_{ax}$ CT state is only slightly reactive, if at all. It follows that the inefficient photoreaction of $[W(CO)_4(en)]$ under 458 or 476 nm irradiation[18] is either a thermally activated process from a vibrationally relaxed a^3B state or it occurs from the corresponding singlet a^1B state which is still optically populated at 458−476 nm because of overlapping absorption bands, see Figure 3. Indeed, the singlet a^1B $W(CO_{eq})_2 \rightarrow CO_{ax}$ CT state is much more reactive than the corresponding triplet, as is manifested by the much higher quantum yield, 0.068 or 0.050, measured using irradiation at 366 or 405 nm, respectively.[18]

Complexes containing an electron-accepting α-diimine ligand $[M(CO)_4(\alpha\text{-diimine})]$ have a M → diimine MLCT lowest excited state.[3,4] They show a double emission, both in solution and low-temperature glasses.[10,19] The low-energy emission originates in triplet M → diimine MLCT excited state(s) as was confirmed by triplet TD-DFT calculations of $[W(CO)_4(phen)]$ and $[W(CO)_4(tmp)]$.[17] The high-energy emission of $[M(CO)_4(\alpha\text{-diimine})]$ can now be attributed to spin-triplet $M(CO_{eq})_2 \rightarrow CO_{ax}$ CT state(s), instead of the traditional assignment to ^{3}LF states. Herein, it was found that the high-energy emission of $[W(CO)_4(^t\text{Bu-DAB})]$ originates in $W(CO_{eq})_2 \rightarrow CO_{ax}$ CT states b^3B_2 and b^3B_1. Similar assignments have been made[17] for $[W(CO)_4(phen)]$ and $[W(CO)_4(tmp)]$. The involvement of ^{3}LF states in the emission of $[W(CO)_4(en)]$ and $[M(CO)_4(\alpha\text{-diimine})]$ complexes is convincingly ruled out by the absence of ^{3}LF excited states at spectroscopically relevant energies, as revealed by triplet TD-DFT calculations. It should be also noted that the occurrence of separate emissions from M → diimine and $M(CO_{eq})_2 \rightarrow CO_{ax}$ CT excited states and the distinct photoreactivity patterns observed upon visible and near-UV irradiation indicate that these two states are hardly coupled.

The $d(\pi) \rightarrow d(\sigma^*)$ LF excited states of mixed-ligand metal carbonyls are found to be spectroscopically and photophysically much less important than it is usually assumed. The d-character is blurred by an extensive delocalization that spreads the d-contributions between many more molecular orbitals than predicted by LF d-orbital splitting. Even the three, essentially d_π, highest-lying occupied MOs are less than 60% d in character. Moreover, the σ^* orbitals with any appreciable d contribution and, thus, excited states with at least a partial $d(\pi) \rightarrow d(\sigma^*)$ character occur at very high energies. The LF-like states thus lie too high in energy to be populated by irradiation with visible or near UV light, or even thermally from long-lived MLCT excited states. Nevertheless, $d(\pi) \rightarrow d(\sigma^*)$ LF-like excited states can play an important photochemical role because they interact with lower-lying CT excited states along photochemical reaction coordinates, rendering them reactive.[4,15,27,28,75,76]

The main conclusions of this work, that is, the important spectroscopic, photochemical, and photophysical roles of $M(CO_{eq})_2 \rightarrow CO_{ax}$ CT excited states and the limited validity of ligand field arguments, are probably applicable to many other mixed-ligand carbonyl complexes, including $[CpM(CO)_n]$ complexes[77] that are important[78−83] in photochemical C−H bond activation.

Acknowledgment. J. Jirkovský (J. Heyrovský Institute) and Peter Groen (University of Amsterdam) are thanked for measuring the diffuse reflectance and resonance Raman spectra, respectively. Valuable discussions with C. Daniel (CNRS Strasbourg) and D. J. Stufkens (University of Amsterdam) are appreciated. P. Matousek (CLRC, Rutherford Appleton Laboratory) is thanked gratefully for his help with the measurements of the picosecond time-resolved IR spectra. This technique was developed at CLRC by M. Towrie (CLRC), A.W. Parker (CLRC), and M. W. George (University of Nottingham) whose technical advice is also much appreciated. Funding from EPSRC, Ministry of Education of the Czech Republic, and the COST Action D14 is gratefully acknowledged.

Supporting Information Available: DFT calculated bond lengths and angles, calculated atomic coordinates, and time-resolved IR spectrum (PDF). This material is available free of charge via the Internet at http://pubs.acs.org.

JA021022J

(73) Balk, R. W.; Stufkens, D. J.; Oskam, A. *Inorg. Chim. Acta* **1979**, *34*, 267−274.
(74) Balk, R. W.; Stufkens, D. J.; Oskam, A. *Inorg. Chim. Acta* **1978**, *28*, 133−143.
(75) Farrell, I. R.; Vlček, A., Jr. *Coord. Chem. Rev.* **2000**, *208*, 87−101.
(76) Vlček, A., Jr.; Víchová, J.; Hartl, F. *Coord. Chem. Rev.* **1994**, *132*, 167−174.
(77) Hu, Z.; Boyd, R. J.; Nakatsuji, H. *J. Am. Chem. Soc.* **2002**, *124*, 2664−2671.
(78) Bromberg, S. E.; Lian, T.; Bergman, R. G.; Harris, C. B. *J. Am. Chem. Soc.* **1996**, *118*, 2069−2072.
(79) Bromberg, S. E.; Yang, H.; Asplund, M. C.; Lian, T.; McNamara, B. K.; Kotz, K. T.; Yeston, J. S.; Wilkens, M.; Frei, H.; Bergman, R. G.; Harris, C. B. *Science* **1997**, *278*, 260−263.
(80) Asbury, J. B.; Ghosh, H. N.; Yeston, J. S.; Bergman, R. G.; Lian, T. *Organometallics* **1998**, *17*, 3417−3419.
(81) Purwoko, A. A.; Lees, A. J. *Inorg. Chem.* **1995**, *34*, 424−425.
(82) Purwoko, A. A.; Lees, A. J. *Inorg. Chem.* **1996**, *35*, 675−682.
(83) Dunwoody, N.; Lees, A. J. *Organometallics* **1997**, *16*, 5770−5778.